Faculty of Natural Science and Technology
Department of Physics

MASTER'S THESIS FOR

STUD. TECHN. KNUT MAGNUS

Thesis started:	01.21.2008
Thesis submitted:	14.07.2008

DISCIPLINE: COMPLEX MATERIALS

Norsk tittel:	*"EKSPERIMENTELL FORSKNING PÅ SPREKKDANNELSE I GELER"*
English title:	*"EXPERIMENTAL RESEARCH ON FRACTURES IN GELS"*

This work has been carried out at the Departement of Physics, under the supervision of Professor Jon Otto Fossum.

Trondheim, July 14th 2008

Jon Otto Fossum

Responsible supervisor

Professor at Department of Physics

Abstract

This report describes an experimental study of fractures in Laponite gels using a peel-test like method. A strip of filter paper is placed on top of a sample of Labonite gel. The filter paper absorbs water from the gel and tightly adheres to it. One end is then pulled upwards, causing a layer of the Laponite gel to be peeled off as a fracture propagates horizontally through the sample. To pull the filter paper upwards, a computer-controlled positioner is used, making it possible to control the velocity at which the filter paper is pulled upwards, thus controlling the velocity of the fracture propagating through the sample.

The goal of this study is to investigate properties of the fracture surface, or more specifically to study the roughness of the fracture surface, and to investigate possible correlation between the roughness of the fracture surface, and the propagation velocity of the fracture. An effort has also been made to study the roughness of the fracture front by taking photographs of the samples while undergoing fracture. This effort has however, only been partly successfull. This work is in many aspects a continuation of the work done by Christian A. Nielsen in his Master's thesis [1].

Preface

This thesis is written for the Master degree in Physics (Sivilingeniør) at the Norwegian University of Science and Technology (NTNU). The project was done at the Complex Materials Group at the Department of Physics as a continuation of the preparations made in the course TFY 4705 during the autumn 2007. This project has lasted from January to July 2008.

I would like to thank Professor Jon Otto Fossum, acting as my academic supervisor, for assisting me in this project. In addition I would like to thank Gary Chinga for providing me with laser profilometry measurements. I also want to express my appreciation of the helpful suggestions made by other students and staff at the Department of Physics.

Trondheim, July 14th 2008 Knut Magnus

Contents

List of Figures

Chapter 1

Introduction

For the last century there has been a lot of research on fracture mechanics, but mainly in solid materials, while there has been less focus on fractures in soft materials. There has however been an increasing interest of fractures in soft materials more recently, because of the increasing use of soft materials like plastics and polymers over the last decades.

One type of soft material is clays, which has been used by people for thousands of years. Clays have been used as construction materials and for pottery. Some more modern examples of applications are the use of clays as oil drilling fluids, and as gelling agents, e.g. in tooth pastes and detergents. Recently, clays have gained interest from material physicists because of the increasing availability of clean chemistry customized synthetic clays and this has become an important part of modern materials science.[2]. The study of fracture properties of clay gels is thus an interesting scientific area that is relatively new. The most widely studied synthetic clay is laponite [2] and in this project the clay gel that is studied consists of 97% of water and 3% of Laponite RD, hereby denoted as Laponite.

The goal of this study is to continue the work done by Christian A. Nielsen [1] and investigate the fracture properties of Laponite gels. Another important goal is to develop and improve the methods and experimental setup in order to make it possible to obtain accurate results. The experiment was designed to reproduce the peel-test like method used by Tan aka et. al. [3] to investigate fractures in acrylamide gels. This work was started by Christian A. Nielsen as part of his Master's project in the autumn of 2006. This work has been the basis for the methods and setup in this project, and only minor, but still important adjustments has been made to the setup designed by Christian A. Nielsen. The concept of this experiment is that a strip of paper is attached to the top surface of Laponite gel sample of prismatic shape. The end of the filter paper is attached to a positioner above the sample and by moving the positioner upwards at a constant velocity, a fracture will propagate horizontally through the sample at the same velocity.

As the fracture propagates through the sample it will create two mirrored fracture surfaces, one on top of the sample and the other attached to the strip of filter paper. The fracture surfaces may form patterns that reflect the mechanics of the fractures. Thus the fracture patterns, may provide information about the material. The setup may also be used to study the propagation of the fracture front through the material. This is done by placing a camera below the sample and filming or photographing it while the experiment is performed.

This experiment can, with some modifications, be used to study the roughness of the fracture front, but this has not been the focus in this project. An interesting thing to investigate is whether the roughness of the fracture surface depends on the fracture velocity. Another interesting thing to investigate is the possible dependence between the roughness exponent of the fracture surface and the distribution of the force used to make the fracture.

Chapter 2

Theory

It is not straightforward to decide where to draw the line in terms of what theory to include in this report. On one hand, there are many different fields within physics and science that are relevant to the experiments performed, e.g. optics, which is relevant in terms of optimising the light conditions to get satisfying pictures and videos of the fracture front in a clear gel. On the other hand, the focus has mainly been on the practical task of developing and improving the methods and performing the experiment and the data analysis, so in the example mentioned above, the approach was more in the direction of trying different setups and see what gave the best result based on experiences, rather than applying a theory and deduce how to optimize the light conditions. Nevertheless, the most relevant theory is explained in this chapter.

2.1 Laponite

All the experiments described in this report are performed using Laponite RD, which has the chemical formula $\mathrm{Si_8Mg_{5.5}Li_{0.4}H_4O_{24}Na_{0.7}}$ [4]. This is one particular type of Laponite among a whole range of other Laponite types. Laponite sorts under the family of so-called swelling 2:1 clays and is the most widely studied synthetic clay. Figure 2.2 shows the structure of one individual Laponite particle in the dehydrated state[5].

The particles are disk-shaped with a diameter of 25 nm and a thickness of 1 nm [6]. This is a special property of Laponite clays, as most other clays, both natural and synthetic, are polydisperse with micrometer sized particles, in contrast to the 25 nanometer diameter monodispersity of the colloidal platelets of Laponite. The discs have net negative charge and have negatively charged faces, with positively charged edges. This causes an attracting electrostatic force between the edge of one particle, and the face of another particle. This causes the particles to aggregate in a structure known as the “house of cards” structure when forming a gel, sharing charge-compensating positively charged ions (cations). This structure is described in Figure 2.3.

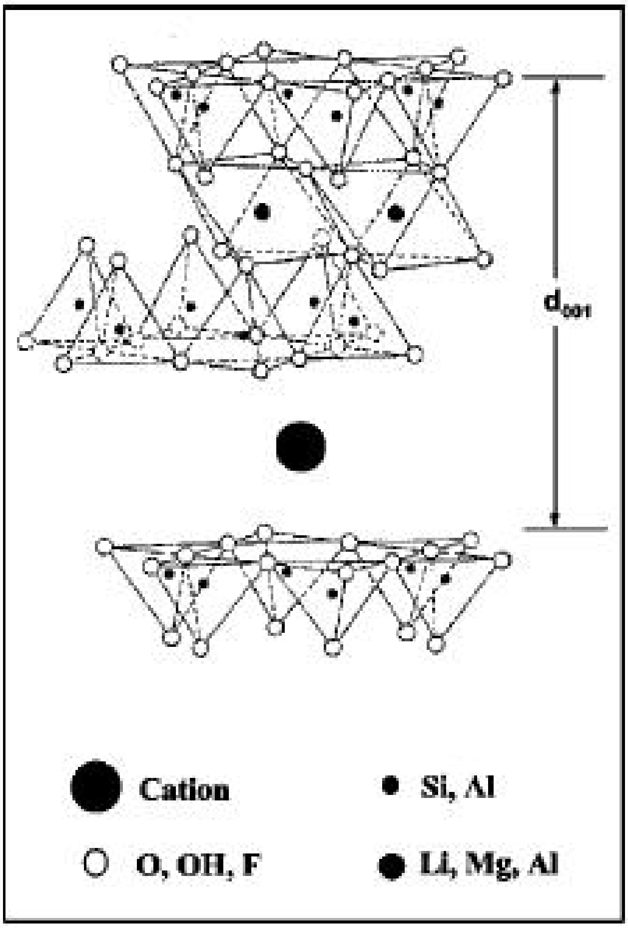

Figure 2.1: The structure of a typical 2:1 layered silicate clay. Laponite contains Na, Si, Mg, Li, O and OH. The basal spacing d_{001} is indicated and below are the symbols for some typical elements of clay components.

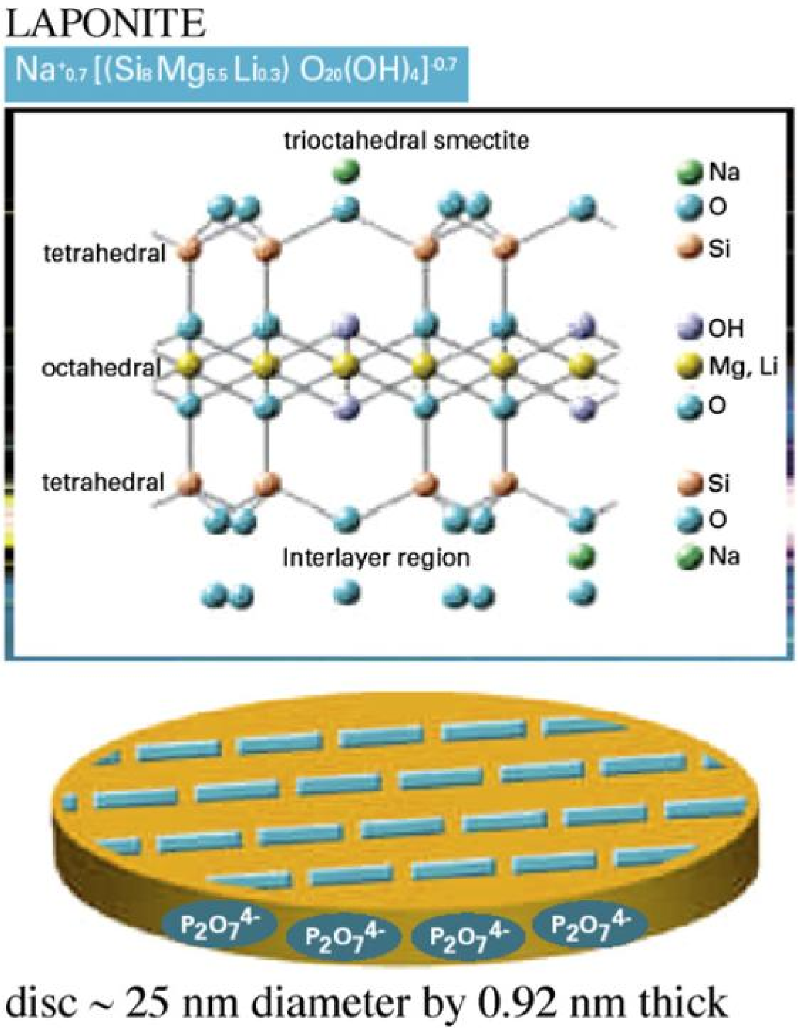

Figure 2.2: The structure of an individual Laponite particle.

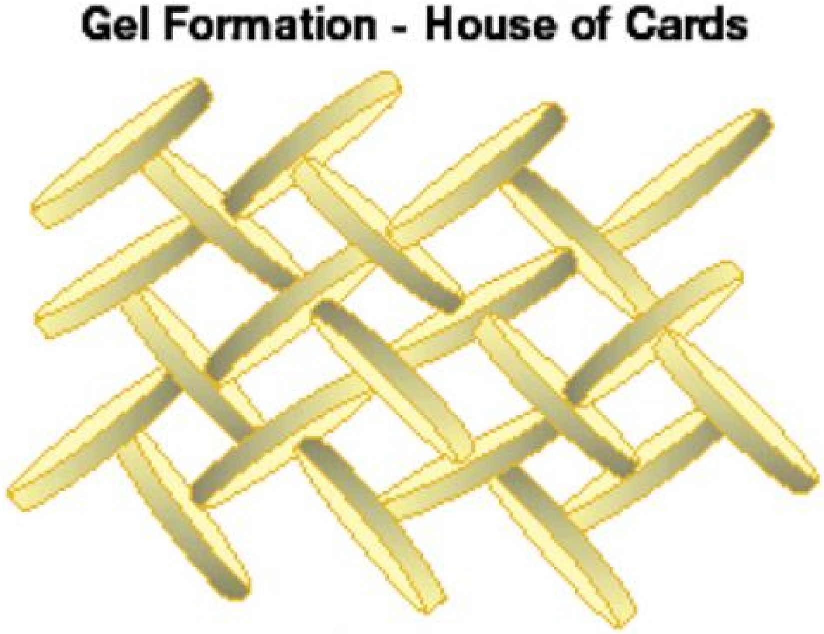

Figure 2.3: The "house of cards" structure of Laponite gel. The electrostatic attraction between the positively charged edges and the negatively charged faces of the discs-shaped colloidal particles, causes the formation of this structure.

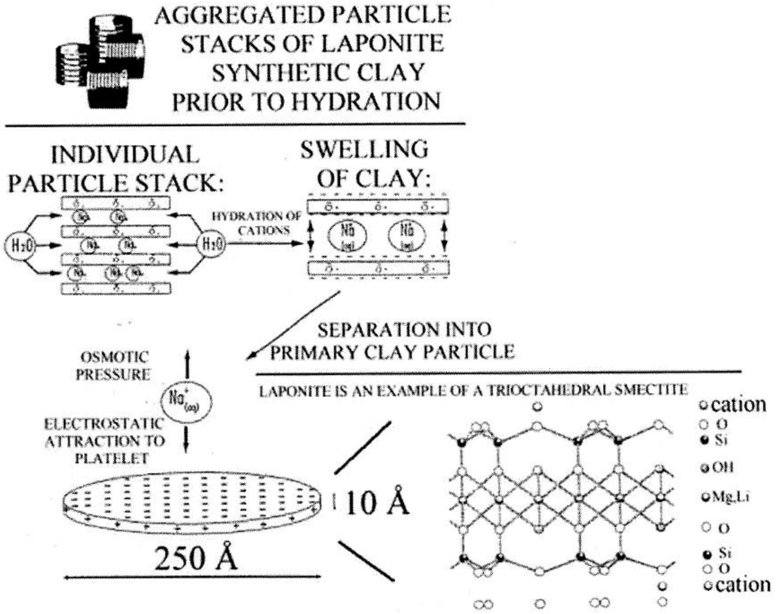

Figure 2.4: The structure of Laponite. In the upper left corner the stacking pattern of a dehydrated particle is shown. In water solutions, water will enter between the individual disks and the ions in the water will interact with the surfaces of the Laponite particles.

2.1.1 Phase Diagram for Solutions of Laponite, Salt and Water

Four phases have been identified experimentally of solutions of clay, salt and water. Figure 2.5 shows these four phases as four regions in the phase diagram, restricted by the concentrations of Laponite and salt. The four regions are the isotropic liquid (IL) region, the isotropic gel (IG) region, the nematic gel (NG) region, and the flocculation (F) region. The reason for this behaviour can be explained by the two different forces that interacts between the particles; the attracting van der Waals force, and the repulsing electrostatic force between the faces of the disk-shaped particles, which are affected by the concentration of electrolytes in the solution. As seen in Figure 2.4 cations in the solution will be electrostatically attracted to the faces of the Laponite particles and this will reduce the electrostatic repulsion between the particles, allowing the particles to get close enough for the van der Waals attraction to keep the particles together.

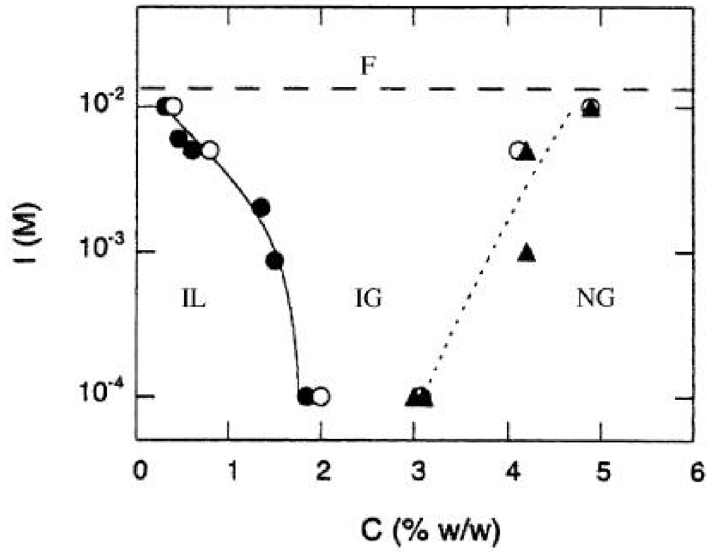

Figure 2.5: Phase diagram for Laponite in a salt-water solution. C is the concentration of Laponite in weight percent. I is the molar concentration of positively charged ions in the solution, which can be changed by varying the concentration of salt (NaCl).

Because of the self protolysis of water, the electrolyte concentration will not be zero when no salt is added to the solution. In this experiment, the gels are made without any salt and with a Laponite concentration of 3 weight percent. The phase of such a solution is an isotropic gel, near the limit of the nematic gel region of the phase diagram.

Isotropic Liquid

In the IL region, smaller groups of platelets form Brownian aggregates, but these aggregates are not large enough to cover any significant portion of the system. The result is dispersed Brownian aggregates suspended in water. No gel is formed and there are no orientational order in the system as a whole. At the lowest concentration the system behaves like a Newtonian fluid and as the concentration of either Laponite or salt is increased, the aggregates become larger and the fluid has ha more complex behaviour. When the concentration of Laponite and salt reaches the transition line between the IL and IG region, the clay concentration becomes sufficiently large for the aggregate structure to percolate. The precise nature of these transitions at various electrolyte concentrations are not known, although dynamic light scattering experiments may be interpreted as being similar to scenarios given by mode coupling theories of structural glass transitions [6].

Isotropic Gel

In the IG region the concentrations of clay and/or salt is large enough for the solution to form a gel. There is still no global orientational preference for the clay platelets, but they are now locked in position in a larger system. According to some experiments the clay platelets form small stacks which in turn form chains that bundle together and form a percolating structure. When the concentration of salt and clay is large enough the system will start to order itself on a global scale. The individual platelets start to form more orientational uniform domains, which again will align themselves with the neighbouring domains, creating a macroscopic orientational preference. There is however little experimental data on this transition.

Nematic Gel

In the NG region there is a macroscopic nematic ordering of platelets. There are to this date few detailed experimental studies of this phase, except at very high clay concentration near dehydration [6].

Flocculation

The concentration of salt is so high that aggregates are no longer Brownian. The aggregates will sediment, giving a clay-water phase separation.

2.2 Fracture Mechanics

Fractures in any material are caused by stress that acts on the material. If a crack has already been initiated in a material subjected to stress, the stress near the crack tip is elevated above the average stress. Stress will build up near the crack tip and the material will eventually fail, allowing the crack to propagate through the material [7].

There are three fundamental ways for forces to act on a material, exposing it to stress, as shown in Figure 2.6. For a Mode I crack, a tensile stress is applied normal to the fracture plane. For a Mode II crack, a shear stress is acting parallel to the fracture plane and perpendicular to the fracture front. For a Mode III crack, a shear stress is acting parallel to the fracture plane and also parallel to the fracture front. Figure 2.6 show pure cracks of Mode I, Mode II and Mode III. In reality cracks are seldom purely one mode, although one mode can dominate. A crack can have a combination of different modes that changes as the fracture propagates.

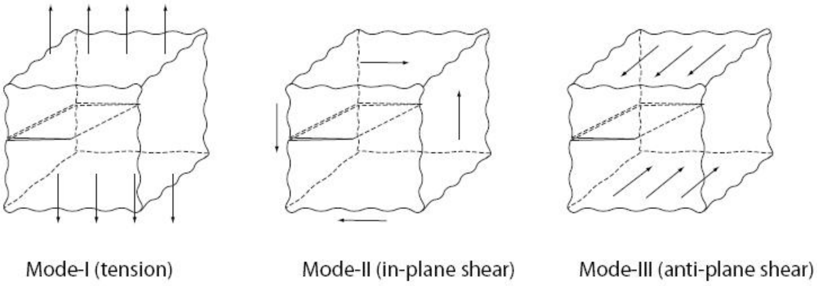

Figure 2.6: The three fundamental types of stress cause three different modes of fracture.

When a crack has propagates through a material, it leaves behind two fracture surfaces. The structural relation between fracture surfaces and crack fronts is studied by Tanaka et. al. [8]. The crack fronts are not straight lines, but consists of many step lines. The actual fracture is an aggregation of crack segments. There is however little known about the fronts of well-developed cracks [8].

Fracture Energy

The energy needed to open a crack depends first of all on how large the crack is. It takes more energy to open a crack in a 20 mm wide sample, than in a 10 mm wide sample. It also takes more energy to let the crack propagate 20 mm through a sample, than to let a crack propagate 10 mm through a sample. In this peel-test like experiment, the energy is supplied by the positioner that pulls the filter paper up, causing the fracture to propagate horizontally through the sample. The force that does the work of the fracture is denoted F. The width of the sample is denoted w. Under the assumption that the fracture front propagates at the same velocity as the velocity of the positioner, which also includes that the force acting from the positioner is always directed vertically upwards, the laws of Newtonian mechanics yields:

$$E = F \cdot \Delta x \tag{2.1}$$

Where E is the work done by a force F causing the fracture to propagate a distance Δx. (2.1) holds only when F and x has the same direction, but in this case, the positioner will move a distance x in the same direction of F when the fracture propagates a distance x horizontally. The material specific fracture energy is denoted G and is not dependent on the width w of the sample. It is obvious that E will be proportional to w because the work needed to open one crack in each of two samples with a width w, is the same as the work needed to open a crack in one sample with a width $2w$. G is also not dependent on Δx. The material specific fracture energy is the same, whether a crack is opened a small distance or a large distance. Obviously, the energy needed to open a crack a distance Δx is proportional to Δx, thus:

$$G = \frac{F \cdot \Delta x}{w \Delta x} = \frac{F}{w} \tag{2.2}$$

This formula is quite intuitive and it makes sense that the energy needed to create a fracture surface of area $w\Delta x$ is proportional to this area. Thus, the energy divided by the area gives the fracture energy which does not depend on the area. G is also called the elastic energy release [3].

2.3 The Roughness Exponent

There is large variety of methods that can be used to estimate the roughness exponent ζ or the Hurst exponent H, as it is also refered to in the literature. In this project, the method used for calculating the roughness exponent is the detrended fluctuation analysis. This method is similar to the variable bandwith method, which involves dividing a profile of length L (i.e. the profile is described by L data points) into one-dimensional "bands" of width Δ and calculating the standard deviation ω of the height h on each band for different bandwidths and for all possible positions of the band on the profile. The bandwidth Δ can be chosen from 1 datapoint up to L datapoints, but all bands of width larger than $L/2$ are discarded because of insufficient independent sampling, as explained by Jean Schmittbuhl et. al. [9]. For self-affine profiles, ω will follow a power law of Δ [10].

$$\omega(\Delta) = \left\langle \left(h(x) - \bar{h}\right)^2 \right\rangle_L^{1/2} \propto \Delta^\zeta \tag{2.3}$$

The detrended fluctuation analysis differs from the variable bandwidth method when it comes to how the bands are analysed. Before the standard deviation of the height for each band is calculated, the linear trend is subtracted for all points in the band. The linear trend is simply the average slope in the band, i.e. the height difference between the final point in the band and the first point in the band, divided by the bandwidth. This method requires more computing power than the variable bandwidth method, but gives more accurate results.

$$\omega(\Delta) = \left\langle \left(h'(x) - \bar{h}'\right)^2 \right\rangle_L^{1/2} \propto \Delta^\zeta \tag{2.4}$$

Other methods used for calculating the roughness exponent, include the second order correlation function, fourier transform of the height-height correlation function, power spectrum density analysis and averaged wavelet coefficients, but due to limited time for the data analysis, only the detrended fluctuation analysis was used and is thus the only method that will be described here.

Chapter 3

Experiment

The experiment can be divided into 3 steps. The first step is to prepare the Laponite samples. The second step is to expose the sample to shear stress, causing a fracture to propagate through the sample. This step also involves recording the applied force, and also recording either videos or photos from underneath. The third step is to analyse the fracture surface and the recorded data from step 2.

3.1 Preparation of Laponite Samples

There are mainly two ways of preparing the Laponite samples and the difference is whether the Laponite is filtered or not. The filtered samples are more complicated to produce, but to obtain accurate results it is necessary to use filtered samples. By filtering the solution, larger aggregations of Laponite particles are removed to ensure that the solution is uniform and homogenous. The unfiltered samples are much easier to produce and they served a big role in this project, as the main focus was to develop and improve the methods and not necessarily to get accurate results.

3.1.1 Unfiltered Samples

The first step of the sample preparation was to fill a beaker with the desired amount of distilled water and putting a magnet inside. The beaker was then placed on a magnetic stirrer which was then turned on. The Laponite powder was then put in a small container standing on a precision scale, using a spoon at first and in the end, to fine tune the amount, using a spattle. This allowed the amount of Laponite to be measured and controlled to make sure the concentration of the Laponite solution reached the desired level. The scale used for this purpose was an Ohaus Navigator N30330 electronic balance. A typical concentration of the unfiltered Laponite samples was 3 %, hence for 0.6 litres of water, 18 grams of Laponite powder was used. When the small container held the correct amount of Laponite powder, it was removed from the precision scale and held above the beaker on the magnetic stirrer. The powder was then carefully added to the water. This was done quite slowly to make sure that the powder didn't form big lumps, because then it would take a longer time for all of the powder to dissolve, due to the reduced surface area in contact with the water. Directly after all the powder was added, the solution was white and opaque. The beaker was left on the magnetic stirrer for approximately 60-90 minutes, until the solution became completely clear and transparent.

The next step of the sample preparation was to prepare the moulds and this was a good way of spending the time needed for the Laponite to dissolve. Each mould consists of 3 parts, showed in figure ref(form); one glass plate of dimensions 160 mm × 40 mm × 2 mm. One aluminium frame with inner dimensions 140 mm × 20 mm × 30 mm, and one rubber gasket used as a seal between the glass plate and the aluminium frame. To avoid leakage between the rubber gasket and the aluminium frame, it was necessary to firmly press them together. For this purpose, regular masking tape was found suitable. Because masking tape is somewhat elastic, it can provide the necessary force without too much trouble applying it. Applying a few firm turns with masking tape in each end, finalised the mould. Some times a leakage was experienced, which of course resulted in that this particular sample was useless, but this was not a big problem, as the usual number of samples prepared was around 10.

When the Laponite was dissolved, the magnet was removed from the beaker and the Laponite solution was poured into the moulds. Each mould was filled up to a level of approximately 2 cm, but this could vary depending on how much of the solution that was available compared to how many moulds that were prepared. During one of the experimental sessions the level was actually varied intentionally in order to investigate the effects of this. After pouring the Laponite into the moulds, they were out inside a sealed container that already contained a hygrometer and a vessel containing a 8% K_2SO_4 solution. This was to ensure a humid environment for the sample, to counteract the evaporation of water from the samples because this would have the unwanted effects of both changing the concentration of Laponite in the samples, as well as deforming the samples, and make the top surface unsuited for the experiment. The samples were left in the container overnight and were ready for the experiment the day after.

3.1.2 Filtered Samples

The preparation of filtered samples was basically done in the same way as with the unfiltered samples as described above. But it diverges in some respects. The basics, as mentioned, are the same: First a solution of Laponite and distilled water is made in a beaker using a magnetic stirrer. But then, before the solution can be poured into the moulds, it has to be filtered and this causes some complications because a solution of 3% Laponite is too thick to pass through the filter, even when using a suction pump to reduce the pressure under the filter. Because of this complication, the initial concentration only was 1%. Then the solution was filtered using a Nalgene filtration unit with a suction pump. The filter used had a pore size of 0.8 μm.

After filtration, the concentration had to be increased by evaporating two thirds of the water. The amount of Laponite would not be affected by this, so the goal was simply to reduce the amount of water in order to increase the concentration of Laponite. The solution was poured into a large lasagna pan with a basal area of approximately 400 mm × 300 mm and a depth of approximately 50 mm. The lasagna pan was weighed in advance, and then it was weighed again after the solution was poured into it. This was to control the concentration of Laponite in the solution. The initial concentration was known to be 1% and assuming that the filtration did not change the concentration significantly, the concentration would still be 1% when poured into the lasagna pan and weighed. This made it possible to calculate the amount of Laponite in the lasagna pan, from the weight of the solution and the concentration. The lasagna pan was then placed inside a heating cabinet where it was exposed to a temperature of approximately 80°C to 100°C and a strong air flow. The heating cabinet that was used, was a Memmert Model 700. This, combined with the large surface area of the lasagna pan that contained the solution, made it possible to reduce the amount of water in the solution by evaporation within a couple of hours, depending on the amount of Laponite solution that was prepared. The pan was repeatedly taken out and weighed, to monitor the concentration of Laponite in the solution. This was done until the weight reach the desired weight W_d given in (3.1).

$$W_d = W_l + \frac{c_i}{c_d}(W_i - W_l) \tag{3.1}$$

Here, W_d is the desired weight of the lasagna pan with its contents. The goal of this process is to achieve this weight, because then the concentration of Laponite will be equal to the desired concentration. W_l is the weight of the lasagna pan, c_i is the initial concentration of Laponite, c_d is the desired concentration of Laponite and W_i is the initial weight of the lasagna pan with its contents. In this experiment, the following parameters were never changed: $c_i = 1\%$, $c_d = 3\%$, $W_l = 0.731$ kg. This means that W_d was always given by W_i according to (3.2).

$$W_d = 0.731\text{kg} + \frac{1\%}{3\%}(W_i - 0.731\text{kg}) = 0.487\text{kg} + \frac{1}{3}W_i \tag{3.2}$$

During the evaporation process it is important to have a large enough amount of the solution, so that the depth in the lasagna pan does not decrease below a few millimetres. If the depth gets too small, there is a big risk that the solution will start forming a gel in parts of the of the solution before the desired concentration is reached. This meant that it was not possible to produce less than approximately 0.5 litres of the solution, meaning that it was necessary to start with at least 1.5 litres of the solution with a Laponite concentration of 1%.

After the evaporation process, the rest of the preparation was done in the same way as with the unfiltered samples. It does however take much longer time for the filtered solution to form a gel, so the samples should be stored in a humid environment for as much as 10 days as done by Cousin et. al.[11], while the unfiltered sample would be ready overnight. This is the reason why the unfiltered samples were used in this project. The aim was not to get accurate results, but to develop and improve the method, so it was convenient to employ the method that required least work. It was also convenient not having to wait for 10 days for the samples to be ready, in particular because there was always a risk of something going wrong, ruining some or all of the samples. This happened several times during the project, but most of the problems that have emerged, have already been solved.

3.2 Method

The experiment aims at exposing the Laponite gel sample to shear stress in a controlled way, resulting in a fracture to propagate through the sample. This is done using the same peel-test-like method as used by Tanaka et. al. [3]. The basic idea is to peel off a layer from the top of the Laponite gel sample as shown in Figure 3.1.

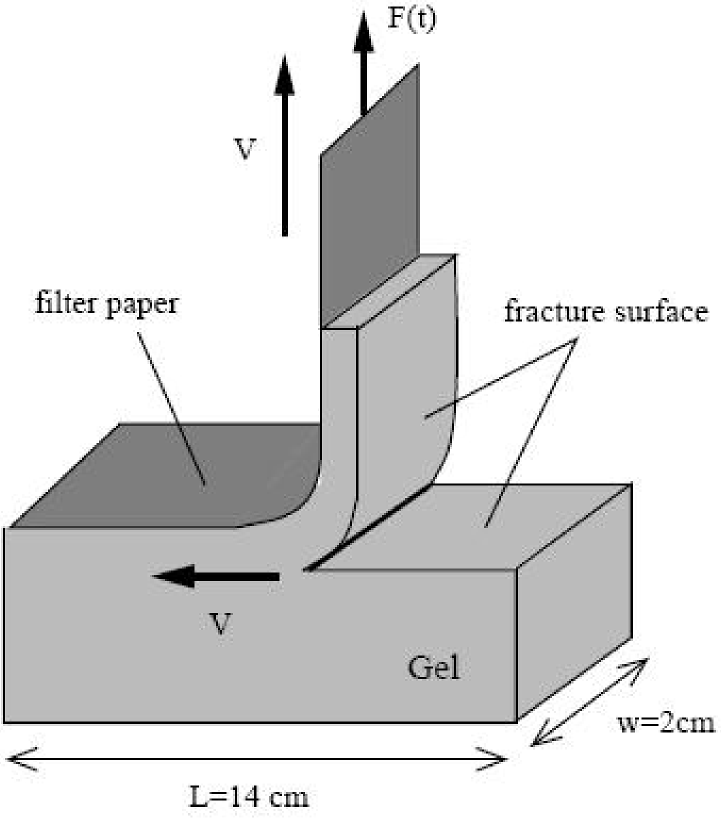

Figure 3.1: A schematic showing how applying a force upwards on the filter paper, results in a fracture propagating through the sample.

This is done by attaching a strip of filter paper to the top surface of the sample and then pull one end directly upwards at a constant velocity v. This will cause a fracture to propagate horizontally through the sample, separating the top layer that follows the filter paper upwards from the rest of the gel in the sample, which remains in its initial position. The fracture will also propagate at a velocity v. During this process, either videos or pictures are taken from directly underneath the sample, in an attempt to investigate the fracture front as it propagates through the sample. The force used to pull off the layer and create the fracture is also recorded, so that the fracture energy can be calculated. Figure 3.2 shows the experimental setup, where the sample is placed on a glass plate, making it visible from directly below. Directly above, there is a positioner that can move vertically. A load cell is attached on the positioner, and a string of approximately 1.6 m is attached to the load cell, making it possible to measure the force used to pull the string, which corresponds to the force used to pull the filter paper up, peeling off a layer of the Laponite gel.

3.2.1 Preparation of experiment

The first step was to remove the aluminium frame. This had to be done carefully to make sure the gel wasn't damaged in the process. The gel would adhere to the inner surface of the frame, so after removing the tape that kept the frame in place, a thin blade was used to separate the gel from the frame by moving it along the inner surface of the aluminium frame. This could normally be done without causing any visible damage to the gel, except from in the immediate vicinity of the edge against the inner surface of the frame.

After separating the outer surface of the sample from the inner surface of the frame, the frame could be lifted directly upwards, making sure the gel didn't stick to it and follow it up. The gel would then stand on its own without noticeably changing shape as a result of gravity, at least not during the time necessary to perform the experiment, which could be as much as half an hour. When the frame was removed, a strip of filter paper was placed on the top surface of the sample. The strips were made by simply cutting out rectangles from circular sheets of filter paper with a pair of scissors, and making a hole in one end using a regular hole puncher. The dimensions of the rectangle were typically 160 mm × 25 mm. The strip had to cover the entire top surface of the sample, which had dimensions 140 mm × 20 mm, and also there had to be room for a hole in one end.

When the strip of filter paper was placed on the top surface of the sample, it would absorb water from the gel, and adhere to the surface after a few minutes. The sample was then placed in position on the glass plate with a camera directly below and with the positioner directly above, as shown in Figure 3.2. The positioner was put in the lowest position, to prepare to move up and pull the filter paper upwards. A paper clip was bent to form a hook, and this was attached to the lower end of the string hanging down from the positioner. This hook was then put through the hole in the filter paper to connect the filter paper to the string.

The experiment is controlled by a computer. The load cell is connected to a computer controlled multi meter, in order to store the force as a function of time during the experiment. This was done using Labview. The positioner was controlled using the program WinPos. To start the experiment, the Labview

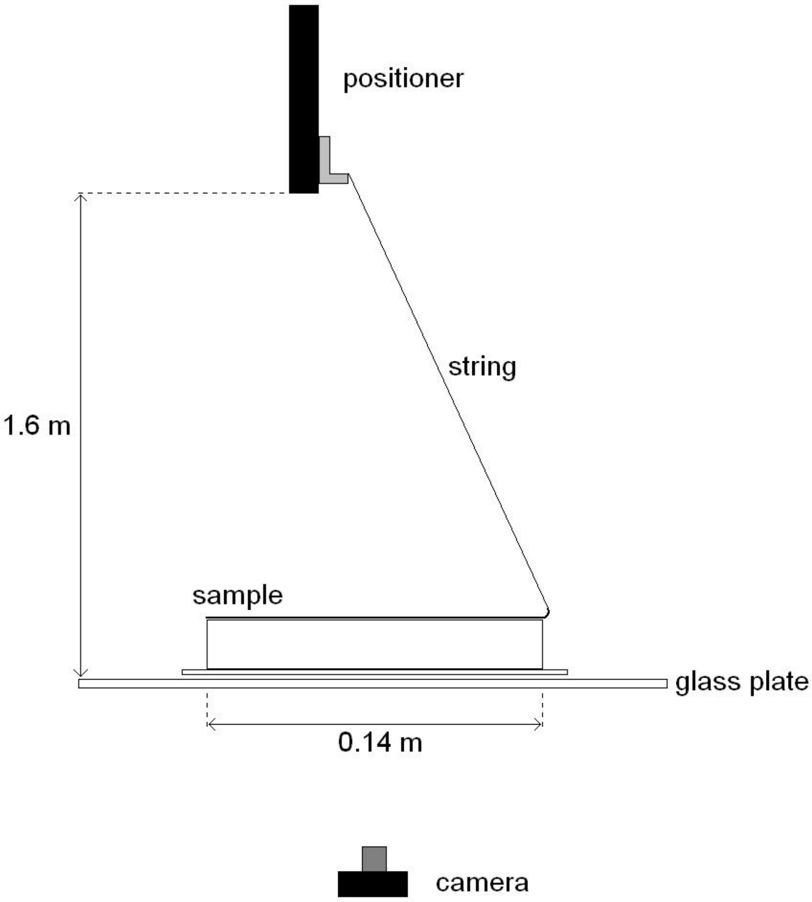

Figure 3.2: The experimental setup, viewed from the side. The VT-80 positioner at the top of the illustration pulls the string upwards, causing the filter paper attached to the sample to peel off a layer from the top of the sample. This makes a fracture front propagate horizontally through the sample. As the fracture progresses through the sample it is filmed or photographed by a camera or video camera directly under the sample.

Figure 3.3: A gel sample with a strip of filter paper placed on the top surface. This picture was taken after approximately 5 minutes and the filter has absorbed water from the sample.

Figure 3.4: A gel sample undergoing fracture. The filter paper is pulled upwards and a thin layer of gel is peeled off the rest of the sample, causing a fracture to propagate horizontally through the sample.

VI was first started to record the force. And then the command to move the positioner upwards was run. It would then be time to start the video camera to record a video of the propagating fracture front. The video camera used for recording videos was a Sony DCR-HC96 DV-camera with a resolution of 720 × 576 pixels. In some cases photographs was taken instead. This was done using a Canon EOS 350D digital mirror reflex camera with a resolution of 8 megapixels. In both cases the camera or video camera was mounted on a Sony camera stand. The auto focus function did not turn out to be suited because of the lack of contrasts to focus on in a transparent gel. Therefore, the focal length was adjusted manually in advance, both for the videos and the photographs.

A substantial effort was put into optimising the conditions for making the fracture front visible. This was done by experimenting with different backgrounds and light sources and by varying the positions and the directions of the light sources. The photographs were then loaded into Photo shop where several parameters such as contrast, brightness, etc. could be varied in the attempt to locate the fracture front.

After the experiment, the fracture surface could be casted using the RepliSet equipment. This was straightforward to use, by simply covering the surfaces with the silicon rubber-compound and wait for a couple of minutes.

3.3 Equipment

The equipment used to in this project is the same as the equipment used by Christian A. Nielsen and is described in his Master's thesis [1]. A representation of the individual parts is given in this section.

VT-80 Positioner

The positioning device used for the experiment was the translation stage 200mm VT-80 from Micos Gmbh. The unit is based upon a back-lash compensated lead screw which produces quiet smooth movement through a DC-, 2-phase-micro-step (SMC-series) motor. The accuracy per 50 mm is ±100 μ m, with a path flatness of ±20 μ m and a velocity range from 0.001 mm/s to 20 mm/s. This positioner can pull loads up to 5 kg and is controlled by computer through a Corvus SMC controller [12].

Figure 3.5: Translation Stage VT-80 positioner.

Corvus SMC Controller

The VT-80 positioner is controlled through a Corvus SMC controller from Micos Gmbh. This unit can be controlled through a computer by the use of the ASCII command language Venus-1. This may be used through either Micros' software Win pos, Labview or Hyperterminal. In this case Winpos was used. The Corvus can control up to three positioners and has a 133 MHz RISC Processor, with Flash-Memory and several alternatives for computer interfacing [12]. In this case the RS-232 serial port was used.

Figure 3.6: Corvus SMC controller [12].

Fracture Surface Replication Equipment

Two fast curing two-component silicon rubber compound called RepliSet F1 and RepliSet G1 was used to cast fracture surfaces. The main difference between these two compounds is that F1 is black and G1 is grey. The material has a minimum resolution of 0.1 μ m, a working life of one minute and a curing time of 4 minutes at room temperature. The material is stored in double chambered cartridges. The compound is applied to fracture surfaces with a dispensing gun which pushes the two compounds from the cartridges through a mixing nozzle. The dispensing gun used is displayed in Figure 3.7 with cartridge and mixing nozzle attached.

Figure 3.7: Dispensing gun for dispensing RepliSet silicon rubber casting compound. A cartridge and mixing nozzle is mounted on the gun.

Cameras

The camera used for photographs was a Canon EOS 350D with the kit lens. This camera has a resolution of 8 megapixels. For video recordings, two different video cameras was used; a Sony DSC-PC110E digital video (DV) camera, and a Sony DCR-HC96 DV camera. Both of these cameras has a resolution of 720 × 576 pixels and the frame rate that was used, was 25 fps in progressive scanning mode. The DV camera was mounted on a tripod and used in conjunction with the usual experimental setup.

Figure 3.8: The Sony DSC-PC110E Digital video camera mounted on a tripod. The camera was positioned below the samples during fracture experiments, filming upwards. The cables seen in the photo is a power cord and a firewire cable. The latter connects the camera to a computer where the fracturing process is recorded with Windows Moviemaker.

Load Cell and Related Equipment

A load cell was used to measure the force applied on the sample by the positioner to create and propagate a fracture. The load cell is a PW4KRC3 single point cantilever bending load cell from HBM with a maximum weight capacity of 0.300 kg. The cell is based upon a bending cantilever with attached Wheatstone bridges. The Wheatstone are bridges under a constant reference excitation voltage and are stretched as a load is applied. As the bridges are stretched, the cell has an outgoing voltage with a linear relationship with the applied load. The excitation voltage was supplied by a GW GPS-1850D voltage source and the outgoing voltage registered by an Agilent 34401A Digital Multimeter. The mulitimeter interfaced with a computer with an USB cable.

In some experiments the data from the load cell may be compared with data from an Ohaus Explorer balance. In these cases the balance was placed below the positioner, and the sample placed on the balance. The balance may be connected to the computer through a RS-232 serial port.

Figure 3.9: The PW4KRC3 single point load cell used to measure the fracture energy of a sample undergoing fracture [13].

Equipment for sample preparation

The samples are mixed in a measuring cup which is placed on a magnetic stirrer. Several different stirrers were used for different samples, though it is unlikely that this had any effect on the prepared samples. The magnetic stirrers used were the Schott SLK3, the Heidolph MR1000 and the Heidolph MR3001 Magnetic Stirrer Hotplate.

Weighing was also done at several different electronic scales. The Laponite for the samples was measured at a Ohaus Navigator N30330 with a division $d = 0.002$ g. For measuring the trays used for water evaporation from the Laponite mixture a more sturdy weight was required. Here a Sartorius CP 6201 balance was used. This balance has an accuracy of 0.1 g and a standard deviation of ±0.1 g. The Sartorius CP 6201 was also used for measuring the K_2SO_4 used to keep a high constant humidity in the sample storage container.

After the sample mixture was prepared it was poured into smaller moulds. These rectangular moulds were made in aluminium at the precision engineering workshop at NTNU and had internal dimensions 140 mm×20 mm×30 mm. The moulds were open in the bottom and were placed on a glass plate to allow the Laponite mixture to bond with a glass surface while the mixture sets. The glass plates were ordinary glass and had dimensions 160 mm ×40 mm ×2 mm.

Figure 3.10: The three parts of a mould; glass plate, rubber seal, and aluminium frame.

The seal used between the aluminium and the glass was a simple 2 mm thick rubber mat cut after the shape of the mould. This arrangement worked well as long as sufficient pressure was applied on the rubber seal using ordinary masking tape.

Figure 3.11: From the left: The Heidolph MR1000 magnetic stirrer and the Ohaus Navigator N30330 and Sartorius CP 6201 electronic balances.

Filtration Unit and Pump

The filtration unit used to remove large particles from the initial 1% Laponite mixture used to create filtered samples was a Nalgene 75 mm Filter Unit. This unit used filter paper with diameter of 75 mm to filter the solution and allowed the attachment of a pump to create a lower pressure below the filter paper to ensure flow through the unit. The filter paper utilized for this purpose was Nalgene filter paper with a pore size of 0.8 μm and a diameter of 75 mm.

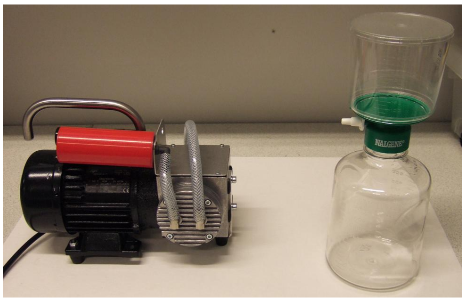

Figure 3.12: The filtration unit (without filter paper) and the pump used to pump the solution through the filter.

Equipment for the Evaporation of the Initial Laponite Solution

In order to ensure a rapid evaporation of the water in the Laponite solution to increase the Laponite concentration the solution was poured into a lasagna pan and put into a heating cabinet. The used heating cabinet was a Memmert Modell 700, in which the solution was subjected to 100 °C and a strong airflow to ensure rapid evaporation. The pan had the dimensions 400 mm ×300 mm ×60 mm.

Sample Storage Container

The samples were stored in a large plastic container with dimensions 400 mm ×30 mm ×22 mm. This container is an ordinary commercial storage container with a loose top which may be attached by two clamps. These clamps press the top firmly against the box frame and thus make the container fairly airtight, although not fully isolated. The box is however sufficiently airtight to keep a significantly higher air humidity inside than outside the container. The high humidity is ensured by placing an open container filled with a 8% solution of K_2SO_4 inside the container. The solution of K_2SO_4 was kept in an open container with a large surface area to ensure maximum evaporation. The humidity was roughly monitored with a simple analogue sauna hygrometer and was constant at about 80%.

Miscellaneous Equipment

The filter paper that was attached to the top of the Laponite samples was circular sheets with a diameter of 240 mm cut into rectangular strips of approximately 160 mm ×25 mm. The paper was Whatman type 4 filter paper.

When the experiments were carried out the samples were placed upon a square 400 mm × 400 mm glass plate above a camera. This glass plate was placed on a simple construction of isopor, which stably elevated the glass plate 120 mm above the surface of the table. This led to the camera lens being approximately 400 mm from the sample, as the camera was standing on the tripod under the table, with the lens pointing upwards. The whole setup was illuminated by a Eligent ELE-WL-ST-1 28W work lamp in some of the experiments, but the best setup was found without the use of this lamp.

Software

The most important computer program for this experiment was the WinPos software. This program controls the VT-80 positioner through the SMC Corvus. Winpos operates through the Venus-1 command language and allows the user to change position, velocity, acceleration and such for the positioner in a simple and efficient manner. The interface of the WinPos software is shown in Figure 3.13.6

Windows Movie Maker was used to import videos of fracture propagation through a firewire connection to the Sony DSC-PC110E DV camera. The DCR-HC96 DV camera does not have a firewire connection on it, but needs a docking station to transfer video to a computer, so the DSC-PC110E camera was found more convenient for this purpose, as the DV-tapes could be switched between the cameras. Labview was also used to design and use a VI (Virtual Instrument) to record the force distribution from the load cell. The interface of the program used to record $F(t)$ for the load cell may be seen in Figure 3.14.

Other utilized software included Matlab and Microsoft Excell for analysis of force distributions.

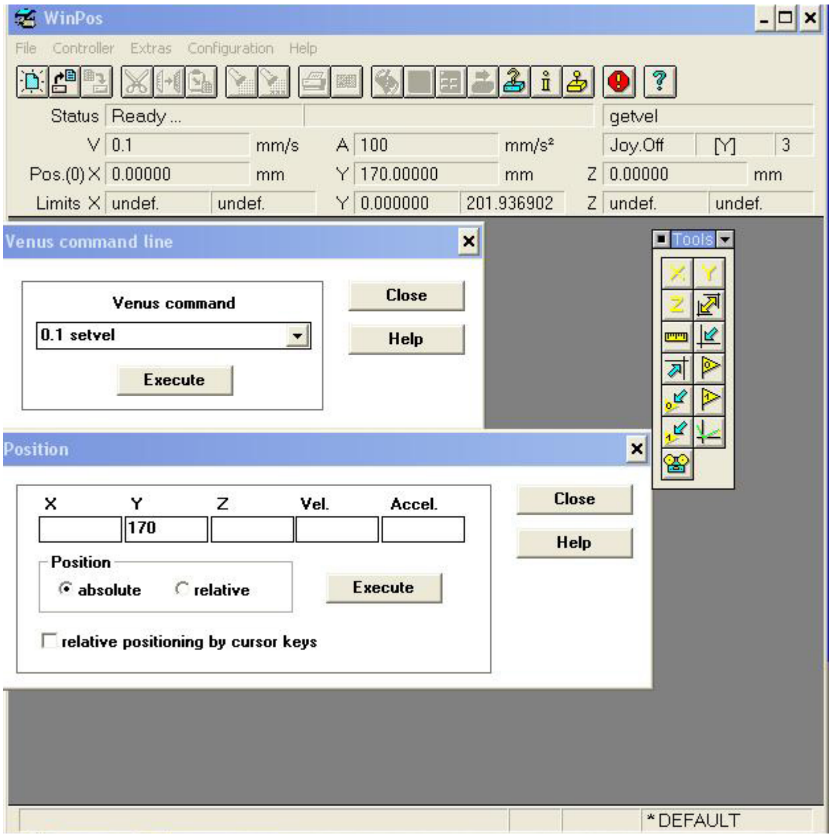

Status Ready ...

getvel

V 0.1 mm/s

A 100 mm/s²

Joy.Off

[Y] 3

Pos.(0) X 0.00000 mm

Y 170.00000 mm

Z 0.00000 mm

Limits X undef. undef.

Y 0.000000 201.936902

Z undef. undef.

Venus command: 0.1 setvel

X	Y	Z	Vel.	Accel.
	170			

Position: ● absolute ○ relative

☐ relative positioning by cursor keys

*DEFAULT

Figure 3.13: The interface of the WinPos software. This software may be used to control the position, velocity and such for the VT-80 positioner. This screen shot was taken before the first test of the experimental setup, and the velocity of the positioner was set to $v = 0.1$ mm/s

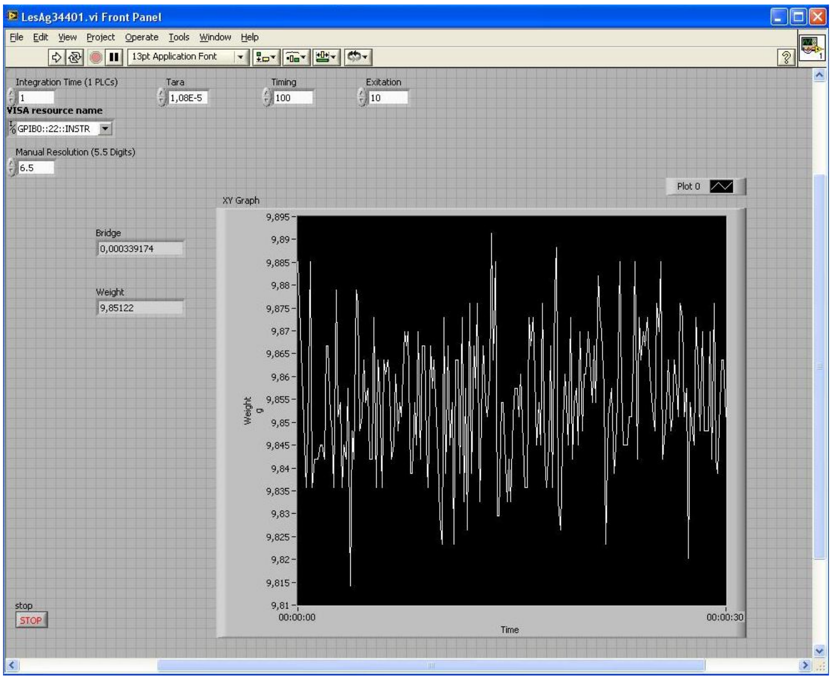

Integration Time (1 PLCs): 1
Tara: 1,08E-5
Timing: 100
Exitation: 10
VISA resource name: GPIB0::22::INSTR
Manual Resolution (5.5 Digits): 6.5
Bridge: 0,000339174
Weight: 9,85122

Figure 3.14: The interface of the Labview program used to record $F(t)$ during fracture experiments. The graph displays the distribution in grams as a function of time.

Chapter 4

Results and Discussion

As mentioned earlier, the focus in this project is not only on the actual studying of fractures in gels, but also on developing and improving the experimental method in order to acchieve accurate results. The methods have been evaluated and through some modifications to the experimental setup, they have also been improved on the course of the project. Consequently, the setup itself will be discussed in this chapter, in addition to the ressults obtained. The methods described and discussed in this report are aimed at obtaining information about the roughness of the fracture surface and the fracture front. The roughness can be described through the roughness exponent ζ, and the goal is to calculate the roughness exponent and determine wheter or not ζ is velocity dependent. Another interesting thing to investigate is the possible relation between the dynamics of the fracture front and the roughness of the fracture surface as discussed by Bouchaud et. al.[14]. Also, the force used to induce the crack will be analysed in order to discover possible relations between the force distribution in time and the fracture surface.

4.1 The Experimental Setup

The first experimental sessions were performed using the same setup as Christian A. Nielsen [1] that was adapted from Tanaka et. al. [3]. The setup was then modified for the rest of experiments in order to increase the accuracy of the experiment.

4.1.1 The Initial Setup

An interesting question regarding this setup is whether it is actually true that the fracture front will propagate with the same velocity as the velocity with which the positioner is set to pull the filter paper up. This will only be an approximation because of the horizontal movement of the fracture front relatively to the (horizontally) stationary positioner. Is this a good approximation? This question should be brought up in order to evaluate the setup used in this project. Another similar question, is whether it is true that the force applied is directed vertically. This is an even more important question, because while the velocity can be calculated in order to compensate for the difference in velocity of the positioner and the velocity of the fracture front, a horizontal component of the force might affect the developing of the fracture and might thus affect the fracture surface aswell. In other words, it is not necessary to use the approximation suggested, that the velocity of the fracture is the same as the velocity of the positioner, but a horizontal component of the force, however, can affect the experiment in a way that could make it necessary to change the setup.

The left schematic of Figure 4.1 describes the setup. Note that the angle θ changes during the process, while the approximation mentioned implies that $\theta = 90^\circ$ at all times. The force is always acting along the string and the filter paper that is already pulled off and acts as an extension of the string.

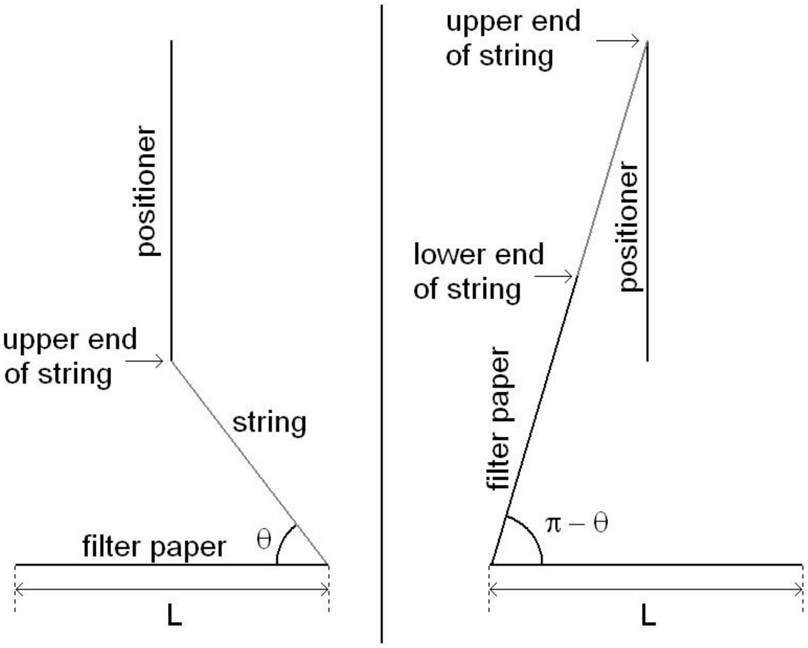

Figure 4.1: Two schematics describing how the system changes during the experiment. The schematic to the left shows how the system looks at the beginning. The filter paper lies on the top surface of the gel, and the positioner is in the lower position. The upper end of the string is attached to the positioner and can only move vertically with the positioner along the vertical line which represents the possible positions of the positioner. The schematic to the right shows how the system looks in the end. The filter paper is pulled up and acts as an extension of the string between the positioner and the fracture front.

A more general schematic is displayed in Figure 4.2 and this will be the basis of the discussion that follows.

The distances s and x of Figure 4.2 is assumed to be equal according to the approximation. This is a good approximation only when the length of the string R is much larger than the length of the sample L. The velocity $v_f = \frac{\mathrm{d}x}{\mathrm{d}t}$ of the fracture front will then be a function of R, L and the velocity $v_p = \frac{\mathrm{d}s}{\mathrm{d}t}$ of the positioner. In this experiment, L is approximately 0.14 m and R is approximately 1.6 m. It is then possible to calculate how big error the approximation gives.

The positioner's height above the sample is denoted y and is, as Figure 4.2 implies, $y = h + s$. (4.1) is obtained simply by applying The Pythagorean Theorem to the right-angled triangle with cathetus $\frac{L}{2} - x$ and y and with hypotenuse $R + x$, as it appears from Figure 4.2

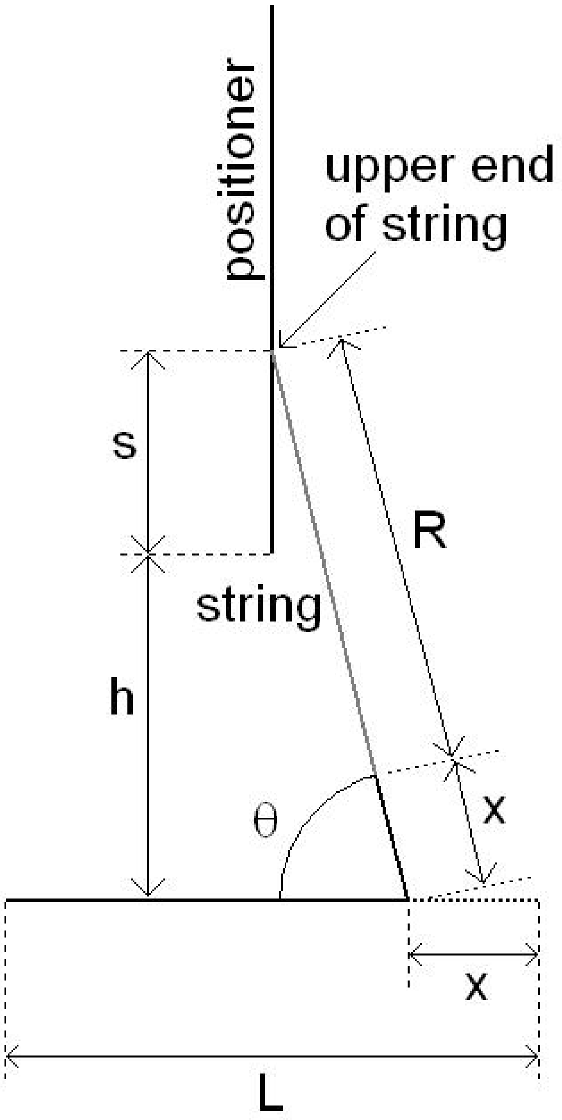

Figure 4.2: Schematic showing the system during the experiment. Here, the positioner has moved up a distance s, and the fracture has propagated a distance x from the starting point.

$$y^2 + (\frac{L}{2} - x)^2 = (R + x)^2 \tag{4.1}$$

(4.1) can then be simplified and y and x can be put on each side of the equal sign:

$$y^2 + \frac{L^2}{4} = R^2 + (2R + L)x \tag{4.2}$$

The time derivative of (4.2) is:

$$2y\frac{\mathrm{d}y}{\mathrm{d}t} = (2R + L)\frac{\mathrm{d}x}{\mathrm{d}t} \tag{4.3}$$

Because $y = h + s$ and h is constant, $\frac{\mathrm{d}y}{\mathrm{d}t} = \frac{\mathrm{d}s}{\mathrm{d}t} = v_p$. Thus, by (4.3) the following expression is obtained:

$$v_f = \frac{2(h + s)}{2R + L}v_p \tag{4.4}$$

as $v_f = \frac{\mathrm{d}x}{\mathrm{d}t}$

h can be expressed by R and L as (4.5) and with $R = 1.60$ m and $L = 0.14$ m inserted into (4.5):

$$h = \sqrt{R^2 - \frac{L^2}{4}} = 1.5985m \tag{4.5}$$

This means that the difference between R and h is only 1.5 mm. This is less than the accuracy of the measurement of R, and $h = R$ is a good approximation. The largest deviation from the approximation will occur in the beginning and in the end of the experiment when $\frac{L}{2} - x$ has the largest absolute value. The relative velocity difference $\frac{v_f}{v_p}$ is then given by (4.6).

$$\frac{v_f}{v_p} = \frac{2(h + s)}{2R + L} \tag{4.6}$$

In the beginning, when $s = 0$, the relative velocity difference will be 4.28%. In the end, $y = \sqrt{(R + L)^2 - \frac{L^2}{4}}$ thus $s = y - h = \sqrt{(R + L)^2 - \frac{L^2}{4}} - 1.5985\mathrm{m} = 0.14009$ m. So the relative difference $\frac{v_f}{v_p}$ is then 4.20%. When the angle θ is at its extreme values, then $\cos\theta = \frac{0.07m}{1.6m} = 0.044 \Longrightarrow \theta = 87.5°$ and $\sin 87.5° = 0.999$.

This means that the error made by using this approximation is a few percent. The consequences of these errors are that the fracture propagates with a velocity that is not constant, although the variation is quite small. Further, the force applied is not vertically directed, except from half way through the experiment, but it varies between 87.5° and 92.5°. Thus the vertical component of the force deviates from the total force by 0.1%. The horizontal component is assumed to be zero, but it actually reaches 4.4% of the measured force at the most. In the beginning, this component is directed forward, in the same direction as the fracture propagates. In the end, the horizontal component of the force is directed backwards. If necessary, the distance h and the length R of the string can be increased in order to reduce the effects discussed above. This is an important evaluation, not because it is convenient to use the approximations $\theta = 90°$ and $v_f = v_p$, but because a horizontal component of the force may affect the results in an unknown way. As described in Section 2.6, the fracture will not be a pure Mode I crack. The horizontal component will also cause some degree of in-plane shear, so the fracture will be a combination of Mode I and Mode II.

4.1.2 The Modified Setup

Because the fracture propagates horizonatally, the filter paper is not pulled directly upwards at all times using the initial setup, as explained above. Also, the propagation velocity of the fracture is not constant because of this horizontal movement. To acchieve a vertically directed force at all times, it is necessary that the positioner follows the fracture's horizontal movement at the same time as it pulls the filter paper upwards. This will ensure that the fracture velocity v_f is constant at all times, as long as the positioner velocity v_p is constant. This horizontal movement can be acchieved by tilting the positioner at an angle of 45 degrees. Then it will have a horizontal velocity component that is equal to its vertical velocity component and the force will act directly upwards at all times. It is necessary, in order to avoid a loss in accuracy of the force measurement, to turn the load cell 45 degrees the oposite way relatively to the positioner so that the load cell has the same orientation as before, as shown in Figure 4.3. The reason for this, is that the load cell only measures the vertical component of the force. If the load cell is tilted, the signal-to-noise ratio will drop by a factor $\frac{1}{\sqrt{2}}$.

To make this change to setup, the beam on which the positioner was mounted in the ceiling, and the bracket that was mounted on the moving part of the positioner, holding the load cell, was taken down and new holes were made in the mechanical workshop to allow the mounting of the positioner at an angle of 45 degrees.

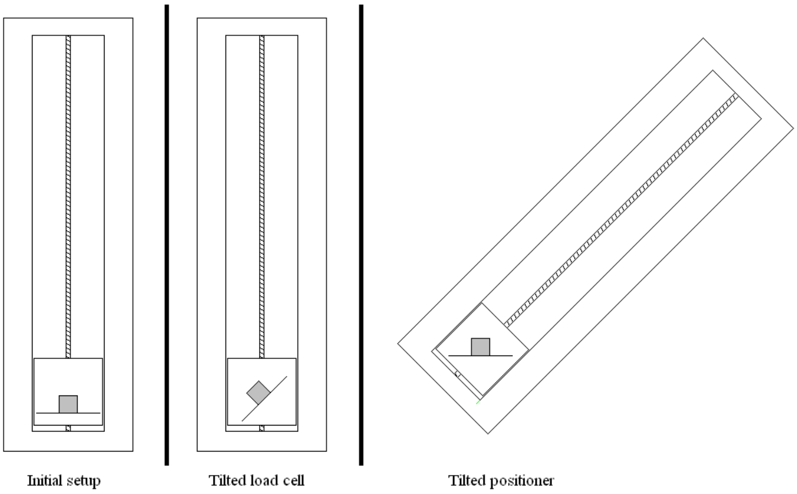

Figure 4.3: Schematics showing the improved setup. The modifications to the positioner setup was done by tilting the load cell realtive to the positioner and then tilting the positioner relative to the sample underneath it. The load cell's orientation remains the same as before.

As a consequence of this modification to the setup, some small new issues emerged. The modified system is less flexible in terms of the length of the string and the positioning of the filter paper on the sample. With the initial setup, the length of the string could vary within 0.06 m because the positioner can move roughly 0.21 m, while the length of the sample is only 0.14 m. With the modified setup, however, the positioner's vertical movement is reduced by a factor $\frac{1}{\sqrt{2}}$, which is equivalent to roughly 0.15 m movement in each of the horizontal and vertical directions. For this reason, the length of the string has to be adjusted quite accurately. The same applies for the positioning of the filter paper on the sample as the end of the filter paper acts as an extention of the string.

When adjusting the setup correctly, there is some room for adjusting the position of the sample in order to ensure the string to be vertical, due to the fact that the sample is slightly shorter than the range of the positioner. By looking at the string from a distance and comparing it with a background that is vertical, for instance a door or a bookcase or simply another string with a weight in the end, the sample can easily be placed directly under the positioner with an error of less than 1 cm. Of course, the positioner has to be adjusted as well during this process to ensure that the string is tight. If not, the string will not be vertical when it is tightened by the positioner because of the horizontal movement of the positioner.

Figure 4.4 shows how the system looks when the sample is placed a distance F away from the correct position, i.e. the position where the string is vertical. Note that the misplacement has caused the filter paper to be pulled up before the positioner has moved. As mentioned earlier, it is quite easy to acchieve F ¡ 0.01 m. In Figure 4.4 the proportions are equivavlent to $F = 0.60$ m when the string length is 1.60 m, hence much greater than the realistic misplacement. This is just to make the geometry visible. Of course, the whole point is to place the sample in such a way that it appears that $F = 0$. However, now it better illustrates the errors caused by a misplacement F.

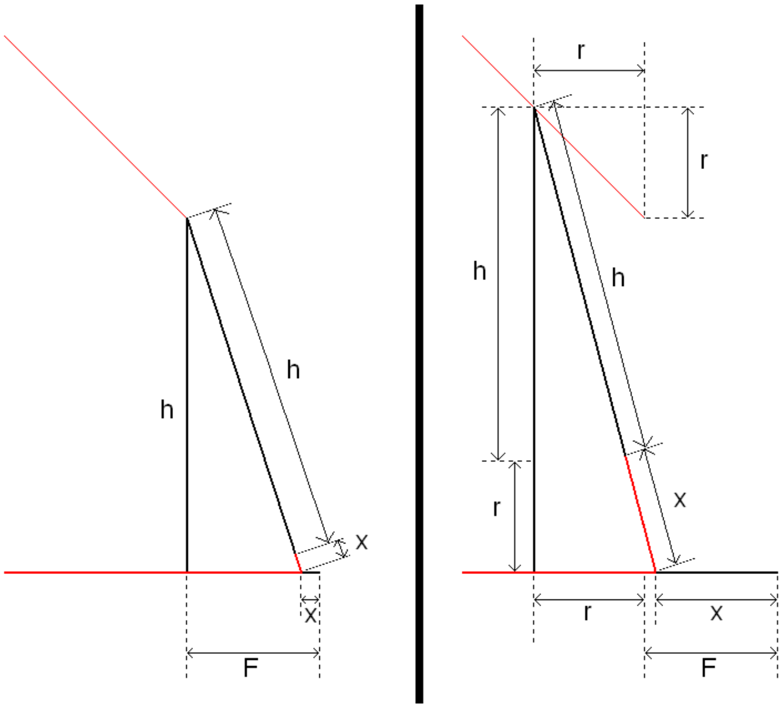

Figure 4.4: Schematics showing the geometry of the improved setup near the end of the sample where the fracture starts. The filter paper is red. The sloping red line at the top represents the positioner and shows where the top end of the string will move. To the left the positioner has not moved yet and the sample has been placed in a position causing the string to slope. The misplacement is denoted F. To the right the positioner has moved a distance r both horizontally and vertically.

The positioner moves with a constant velocity v_p along the red line. This causes the fracture front to move horizontally through the sample with a velocity v_f. The horizontal component of v_p is equal to the vertical component of v_p and from Figure 4.4 it is clear that this is the time derivative of r. Correspondingly the fracture velocity v_f is the time derivative of x, as x is the distance from the end of the sample to the fracture front. If $F = 0$, v_f is equal to the horizontal component of v_p. If $F \neq 0$, v_f can be expressed as a function of v_p.

$$v_p = \sqrt{2}\frac{\mathrm{d}r}{\mathrm{d}t} \tag{4.7}$$

$$v_f = \frac{\mathrm{d}x}{\mathrm{d}t} \tag{4.8}$$

The chain rule yields:

$$\frac{\mathrm{d}x}{\mathrm{d}t} = \frac{\mathrm{d}x}{\mathrm{d}r}\frac{\mathrm{d}r}{\mathrm{d}t} \tag{4.9}$$

Hence, from (4.7) and (4.9)one gets:

$$v_f = \frac{1}{\sqrt{2}} v_p \frac{\mathrm{d}x}{\mathrm{d}r} \tag{4.10}$$

Using the distances given in Figure 4.4 it is possible to find and expression for $\frac{\mathrm{d}x}{\mathrm{d}r}$ by applying the Pythagorean Theorem to the right-angled triangle to the right. Here, the long cathetus is $h + r$, while the short cathetus is $F + r - x$. This triangle is showed explicitly in Figure 4.5.

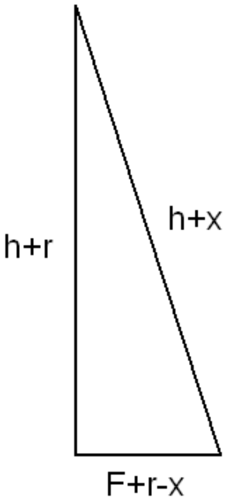

Figure 4.5: The triangle of interest from Figure 4.4

The Pythagorean Theorem yields:

$$(h + x)^2 = (h + r)^2 + (F + r - x)^2 \tag{4.11}$$

By expanding the brackets, one gets:

$$h^2 + x^2 + 2hx = h^2 + r^2 + 2hr + F^2 + r^2 + x^2 + 2Fr - 2Fx - 2rx \tag{4.12}$$

This equation can be simplified by subtracting the terms that appear on both sides and isolate the remaining terms with x on one side:

$$2hx + 2Fx + 2rx = 2r^2 + 2hr + F^2 + 2Fr \tag{4.13}$$

Then x can be expressed as a function of h, F, and r:

$$2x(h + F + r) = 2r^2 + 2hr + F^2 + 2Fr \tag{4.14}$$

$$x(r) = \frac{2r^2 + 2hr + F^2 + 2Fr}{2(h + F + r)} \tag{4.15}$$

A plot of x as a function of r for $r = 0$ to $r = 0.14$ m, is shown in Figure 4.6. Here the misplacement is 0.01 m and $x = r$ is evidently a very accurate approximation. This means that $\frac{\mathrm{d}x}{\mathrm{d}r} \approx 1$ and using this approximation in (4.10), one gets:

$$v_f = \frac{v_p}{\sqrt{2}} \tag{4.16}$$

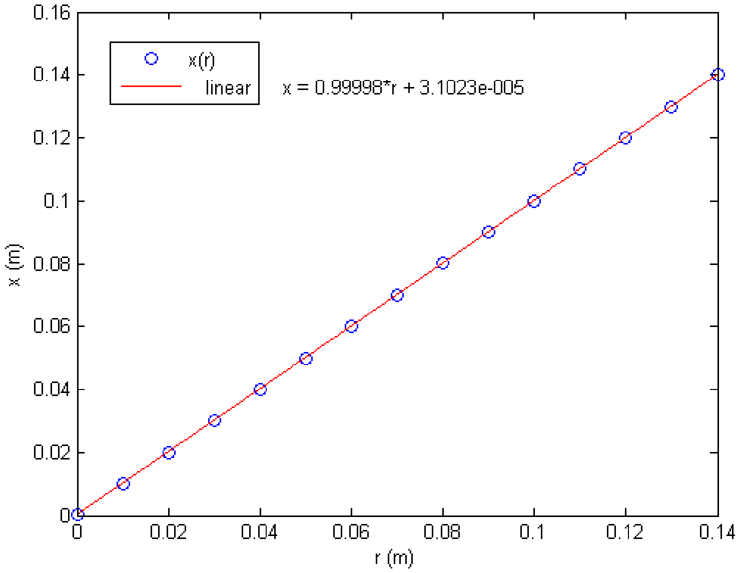

Figure 4.6: x plotted as a function of r with a misplacement $F = 0.01$ m. The blue circles are the points calculated from (4.15), while the red line is a linear fit that shows how close the function is to $x = r$.

To further confirm the above statement, one can find the derivative of the function $x(r)$ from (4.15):

$$\frac{\mathrm{d}x}{\mathrm{d}r} = \frac{4r + 2h + 2F}{2(h + F + r)} - \frac{2r^2 + 2hr + F^2 + 2Fr}{2(h + F + r)^2} \tag{4.17}$$

This function is supposed to be very close to 1. This can be verified by plotting $\frac{\mathrm{d}x}{\mathrm{d}r} - 1$ and ascertain that it is close to zero in the range of r that is used in the experiment. This is shown in Figure 4.7. It is shown by Figure 4.7 that the error is greatest in the beginning and then it becomes smaller as the fracture propagates through the sample. This is a result of the string getting longer as it is extended by the filter paper that already has been pulled up.

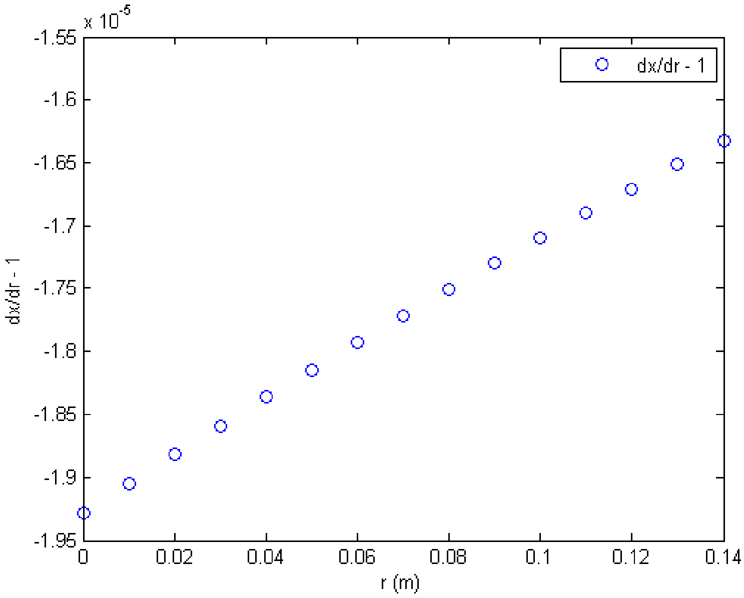

Figure 4.7: $\frac{\mathrm{d}x}{\mathrm{d}r} - 1$ plotted as a function of r with a misplacement F of 0.01 m. The blue circles are the calculated points. The end points which have the values $-1.93 \cdot 10^{-5}$ and $-1.63 \cdot 10^{-5}$ respectively, demonstrates that $\frac{\mathrm{d}x}{\mathrm{d}r}$ is between 0.9999807 and 0.9999837, which is satisfyingly close to 1.

From the above one can conclude that the fracture velocity v_f is very accurately given by (4.16) and it is sufficiently constant for any imaginable purpose, with a misplacement of the sample of 0.01 m or less. It should be added that a misplacement of 0.01 m in the oposite direction will give slightly different numbers than the ones calculated above because the situation is not symmetrical, but as shown in table 4.1 the difference is insignficant.

When it comes to the force, there is a horizontal component f_h that is proportional to the difference between the horizontal components of the position of the positioner and the fracture as shown in (4.18). Figure 4.5 is illustrative in this context as well.

$$f_h = f_v \frac{F + r - x}{h + r} \tag{4.18}$$

Here, f_v is the vertical component of the force, which is measured directly by the load cell. The angle θ between the string and a vertical line (the top angle of the triangle in Figure 4.5), is given by (4.19). $\theta = 0$ is equivalent to $f_h = 0$ which is what this setup is aimed at.

$$\tan\theta = \frac{F + r - x}{h + r} = \frac{f_h}{f_v} \tag{4.19}$$

As shown in Table 4.1, the horizontal component of the force is approximately

Table 4.1: The consequences of different values of F on the fracture velocity and the force. The excact values of the velocity ratio are not interesting beyond the fact that they are very close to either 1 and that they do not change considerably for different values of r.

	$r = 0$		$r = 0.14$ m	
F (m)	$\frac{\mathrm{d}x}{\mathrm{d}r}$	$\frac{f_h}{f_v}$	$\frac{\mathrm{d}x}{\mathrm{d}r}$	$\frac{f_h}{f_v}$
-0.02	0.9999199	-0.0126	0.9999324	-0.0116
-0.01	0.9999802	-0.0063	0.9999833	-0.0058
0	1	0	1	0
0.01	0.9999807	0.0062	0.9999837	0.0057
0.02	0.9999238	0.0124	0.9999354	0.0114

0.6 % of vertical force or less, which is quite satisfying. This means that the fracture will be very close to a pure Mode I fracture.

The total force applied is given by (4.20). The total force is very close to the vertical component, as the angle θ is small. In fact, the relative difference $\frac{f_t}{f_v}$ never exceeds 1.00002 with a misplacement smaller than 0.01 m.

$$f_t = \frac{f_v}{\cos\theta} \tag{4.20}$$

The values of the velocity ratio $\frac{\mathrm{d}x}{\mathrm{d}r}$ in Table 4.1 are obtained by inserting the respective values of F into (4.17). The values of the force ratio $\frac{f_h}{f_v}$ are obtained by inserting the respective values of F into (4.19). Negative value means that the horizontal component of the force is acting in the oposite direction to the direction in which the fracture is propagating.

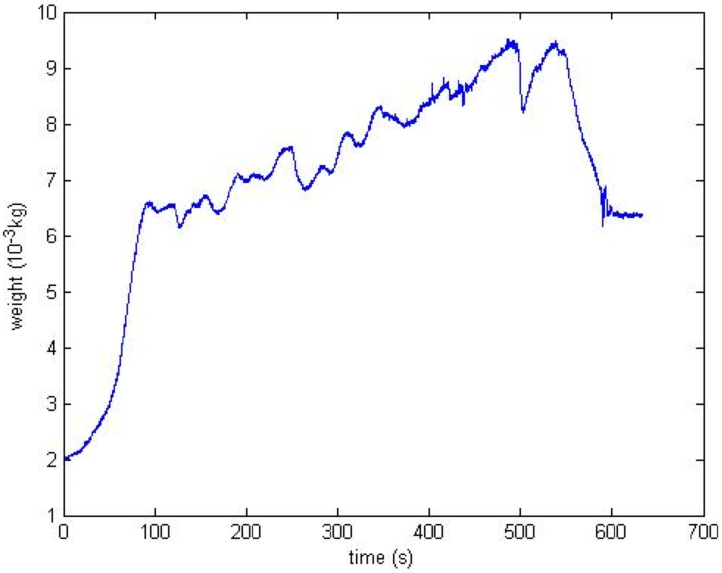

Figure 4.8: Graph displaying the force F measured as a function of time. The units of the force is in kilograms and has to be multiplied with g in order to give the units in N (kg m s^{-2}). There is no fracture until the force is sufficiently large and this happens at t $\approx$ 90 s in this case.

4.2 Fracture Energy

The fracture energy can be found by (2.2). It is, however, not straightforward to measure the force F that is doing the fracture work. The force that is measured with the load cell, is the total force which in addition to F includes the weight of the string and the paperclip hook and the part of the filter paper with a layer of Laponite gel that has undergone fracture. The weight of the string and the paperclip can easily be calibrated for, but the weight of the filter paper with the gel makes it more complicated because this weight is varying in time.

So far, the best approximation that has been found is to assume that the measured force F_m is given by (4.21).

$$F_m = F + \big(m_0 + m(x/L)\big)g \tag{4.21}$$

Here, m_0 is the mass of the string and the paper clip hook, m is the total mass of filter paper with the gel attached to it after the experiment. x is the distance the fracture has propagated and L is the length of the sample. g is the acceleration of gravity. The problem with (4.21) is that it does not take into account that the weight distribution of the filter paper with Laponite gel attached to it, is not necessarily even.

It should be noted that in the beginning (the first 80 - 90 seconds), there is no fracture, and in the end (after about 500 seconds), the force measured is not interesting because the filter paper and the gel directly underneath it is sliding horizontally as the small horizontal component of the force is sufficiently large to overcome the fracture energy of the gel. The graph starts at 0.002 kg as a result of the weight of the string and the paper clip hook.

By using the approximation expressed in (4.21), i.e. subtracting the gravity terms from F_m, the force F can be approximated. The graph will then start and end at 0, which makes sense because the recording of the force was started before the positioner was set to move upwards. It is difficult to tell how much the uneven density per length of the filter paper with gel affects the results. But the fact that the graph drops locally at many different points, indicate that the uneven density is not affecting the results very much. Looking at the average gradient and comparing to the local gradient extremes, it is certainly the pinning-depinning effects, discussed by Daguier et. al.[15] that govern the local variations of the force measured F_m.

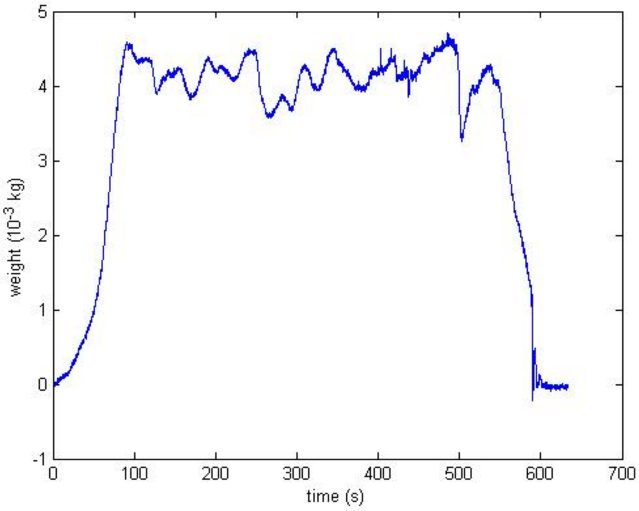

Figure 4.9: Graph displaying the calculated force that is used to open the crack as a function of time.

As Figures 4.9 and 4.10 illustrates, the information acquired towards the end of the experiment is not interesting[1] because the filter paper is gliding horizontally and picking up more gel than before it starts to glide. The step in the end of the graph of Figure 4.10 is just a simple way of marking the point where the weight is increasing more than in the interesting part of the experiment. The behaviour here is not known and also not interesting, but the function has to end up at around 6.4 g because this is the weight that is measured when the filter paper hangs in the string after the experiment.

---

[1] This is actually the case for all the information concerning the last couple of centimetres of the sample because the surface will also be affected by the filter gliding.

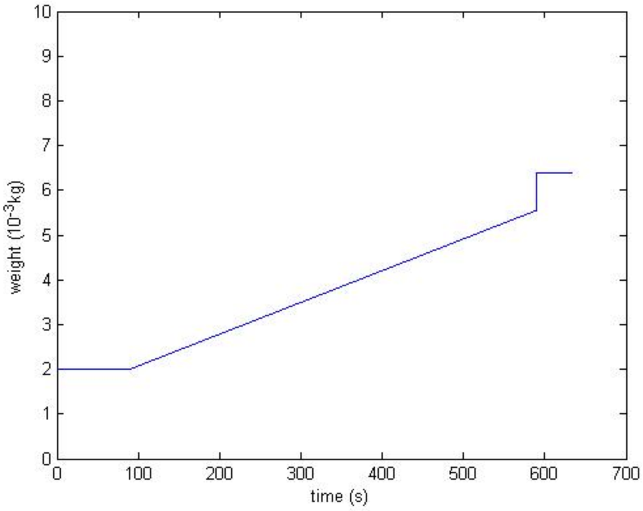

Figure 4.10: The compenstating function that is subtracted from the measured force. The slope is decided using the linear fit function in Matlab. The step up in the end is to compensate for the effects caused by the filter paper gliding horizontally in the end of the experiment.

4.3 The Fracture Front

One of the interesting things to investigate is the possible relation between the dynamics of the fracture front and the roughness of the fracture surface as discussed by Bouchaud et. al.[14]. To study the fracture front of a clear gel is however not an easy task. The only method that was pursued, was by trying to make the fracture front visible.

4.3.1 Videos and Photographs

A substantial effort was put into optimising the conditions for making the fracture front visible. This was done by experimenting with different backgrounds and light sources and by varying the positions and the directions of the light sources. The photographs were then loaded into Photoshop where several parameters such as contrast, brightness and shadows could be varied in the attempt to locate the fracture front. This was a difficult task, as the gel is transparent, like the fracture front. It was also a problem that light was reflected from the fracture surface, as this surface is rough on the cm length scale, and thus reflects light in the direction of the camera no matter where the light came from. It was also a very time-consuming way of working, as Laponite samples had to be prepared for the experiment, and for each sample, the pictures were analysed in Photoshop by manually adjusting the image parameters in the search for a clearly defined fracture front. The camera was more or less in the same position all the time, although some attempts were made to adjust the height of the

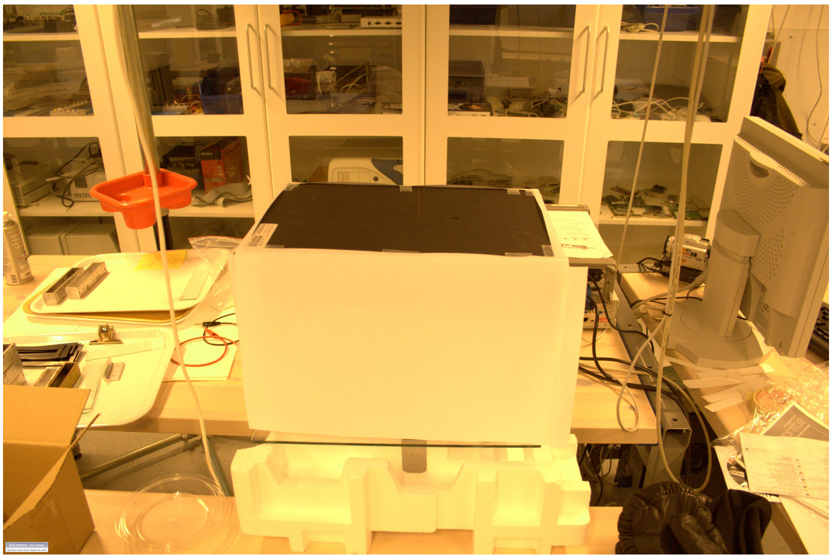

Figure 4.11: The "house" that turned out to give quite satisfying light conditions for photographing the fracture front.

camera in order to increase or decrease the distance to the sample. This had to be combined with adjusting the focal length in order to obtain sharp images. There was however not much room for adjusting the position because of the restrictions of the focal length of the camera, and the proximity to the floor. An office lamp was used to illuminate the sample from various angles, but there always seemed to be a problem with reflections. In most of the attempts, a black paper board was used as background. This had a slit to allow the string that connected the positioner to the filter paper on the sample, to pass through it.

Based on experiences that reflections seemed to cause a lot of trouble, an attempt was made to eliminate or at least reduce this problem. This was done by shading the sample from all light sources with white paper. The idea was to ensure that there was no particular direction from which the light came. The glass plate on which the sample were standing during the experiment was also covered with white paper, but a rectangular hole was cut directly above the camera, where the sample was standing. The result was prismatic shaped "house" with a black ceiling, and white walls and white floor. This turned out to give quite satisfying results. It was also tried for taking videos of the fracture front and this also turned out to be successful. Figures 4.11 and 4.12 show the solution that was found to give quite good conditions for photographing and video recording the fracture front.

Figure 4.13 shows three frames (pictures) from a video recording of the fracture propagation. The dark line is the fracture front and it is clearly changing shape on its way through the sample. This looks promising for future studies.

Figure 4.14 shows a picture where the fracture front can be clearly seen. This photo was taken at a fracture velocity of 0.5 mm/s. There is a bright area

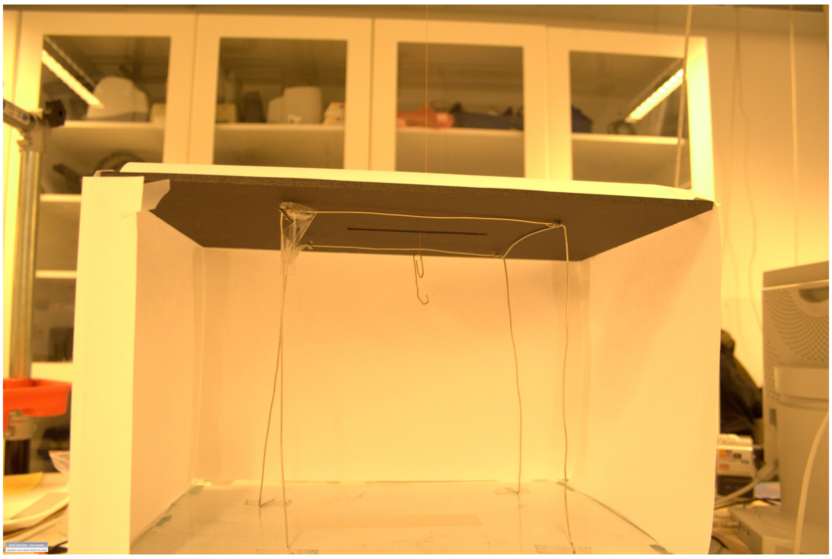

Figure 4.12: The “house” with one of the white walls removed. The sample is placed over the rectangular hole. The string with the hook that is used to pull the filter paper up can also be seen.

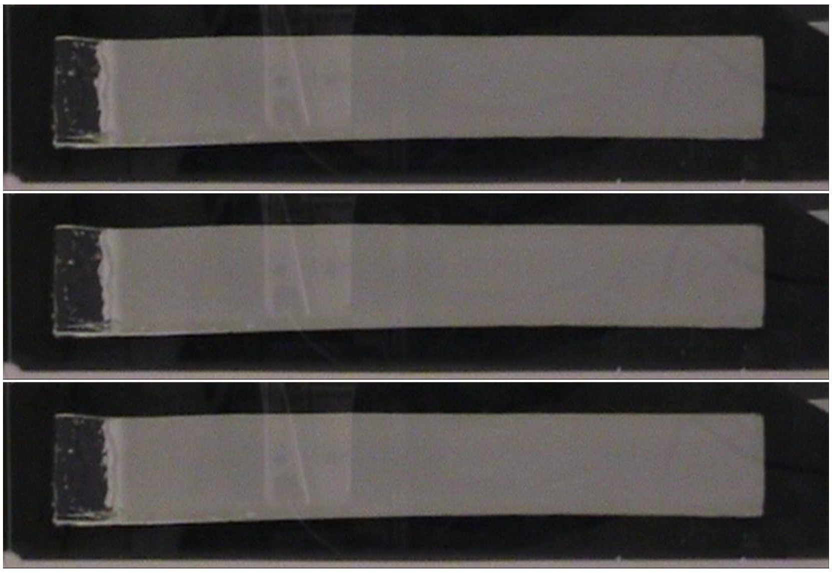

Figure 4.13: Three frames from a video recorded at a fracture velocity of 0.1 mm/s. The frames are taken with approximately 10 seconds intervals. The fracture front is clearly visible and the shape is changing.

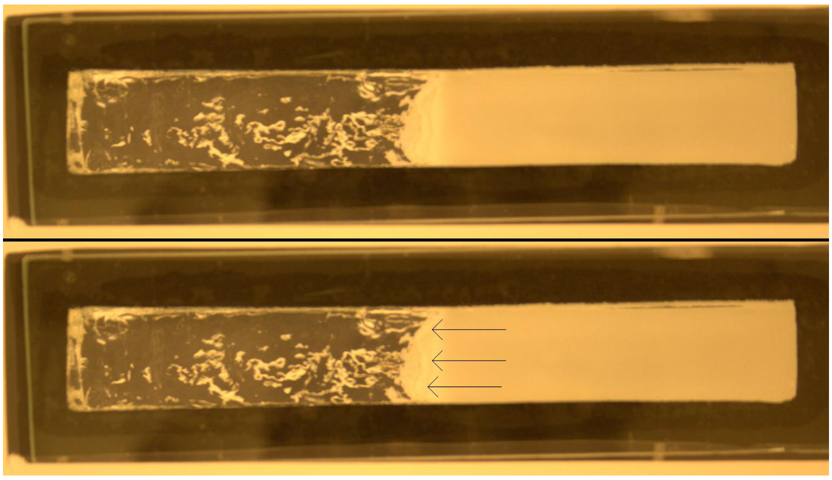

Figure 4.14: Two versions of the same photograph that successfully displays the fracture front. On the top version, the photograph is untouched. On the bottom version the fracture front is pointed to on three different places by the black arrows.

directly in front of and behind the fracture front. In the region in front of the fracture front, the gel is slightly deformed before it yields under the stress and cracks. This means that the filter paper is not lying horizontally in this region, but it is bending upwards. The filter paper will lie horizontally before the fracture front approaches, but then it will be pulled up and hang vertically after the fracture front has passed. The area where the filter paper is bending upwards is illuminated by more light than the area that is facing down towards the camera. Behind this area there is another dark line that looks like the fracture front. This dark line is probably the contour of the gel that is stuck on the filter paper. This surface of the gel that follows the filter paper is also rough and some times this surface will be visible as a dark line. This is in agreements with observations that this second dark line comes and goes during the experiment, but the possibility can not be excluded, that it is cause by some other effect. However, it is obvious that the first dark line is the fracture front, and that is the important information to extract from these photographs.

Figure 4.15 shows a picture where the fracture front is more clearly visible than in Figure 4.14. This photograph was taken at a fracture velocity of 0.1 mm/s, but the main difference from the previous photograph is some small adjustments on the camera and the light conditions. A lamp was placed outside the paper house, behind the fracture front, to the left on the picture. The white balance on the camera was then adjusted untill the fracture front appeared clearly. With this modification, the second dark line didn't appear and another advantage is that the fracture front usually was clearly visible at once, so in most cases it was not necessary to make adjustments in Photoshop. Some times, towards the end of the experiment when the fracture front was close to the other side of the sample, it was not visible before some adjustments were made, but this was still an improvement to the setup.

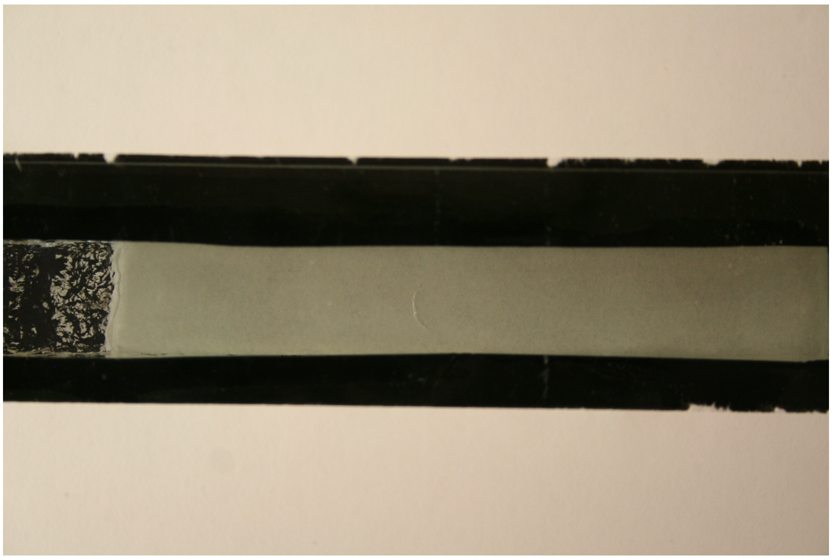

Figure 4.15: Photograph that successfully displays the fracture front. The fracture front is the dark line in the bright area to the left.

Although the photographs made it possible to locate the fracture front, they are not accurate enough for studying the fracture front's roughness. The distance accross the sample is only 20 mm wide and the thickness of the line on the photographs is close to 1 mm. This makes it difficult, if not impossible to say anything about the roughness of the fracture front because of the limited range of length scales that can be studied. This has nothing to do with the resolution of the camera, which is more than sufficient, but it is merely a property of the fracture front. The fracture front is not a sharp edge pointing into the sample, but it is more like a rounded edge gradually, causing the dark line on the picture to be somewhat stretched out. My recomendation for future experiments is to use wider samples in order to obtain a wider fracture front. This may involve some modification to the equipment, but this is necessary in order to study the roughness of the fracture front.

4.4 Fracture Surfaces

In the summer of 2007, some replicas made by Christian A. Nielsen were sent to Strasbourg to be analysed with laser profilometry. However, it turned out that it was difficult to do this analysis, because the surface didn't reflect the light as required for the laser profilometer to work. The surface was said to be too glossy so this gave no results, except that we[2] were advised to find another casting material which was more dim.

A laser profilometer is based on sending light on to the surface from a known

---

[2] In this case "we" refers to the people involved in the project, primarily my supervisor Prof. Jon Otto Fossum and myself.

position and in a known direction, and then detect the light that is reflected in another known direction. The detector is placed behind a slit, to make sure that only light with one specific direction is detected, and the position of the detector is known as well. A line in space is uniquely defined when its direction is given and one point on the line is given. The incoming light can thus be represented by a line in space and the reflected light can be represented by another line in space. Then the height of the surface that is measured, can be found by determining the intersection between these two lines. This intersection will be on the surface, as the reflected light comes from the same point where the incident line hits the surface.

The producer[3] of the casting equipment was contacted and another casting material was ordered, which was specifically recommended for laser profilometry measurements. It turned out that the main difference was that this material had a grey colour instead of black, but the surface seemed to be as shiny and glossy as the material first used.

4.4.1 Gloss of Surfaces

A lot of time was spent wondering about what makes a material or surface shiny or glossy. It was concluded that the surface structure was the deciding factor and thus, changing the casting material, would not help the problem. The resolution of the casting material is 100 nm, which is less than the wavelength of visible light. This should imply that it is the surfaces that is replicated that decides whether the replication surface is glossy or dim. The casting equipment was then used in several small experiments in order to investigate the validity of this conclusion. Most of the surfaces in the lap was replicated and the results most definitely confirmed that the gloss of the replication was decided by the surface that was replicated.

A small area of the of the glass plates used for the Laponite samples was replicated. Figure 4.16 shows the glass plate that was replicated and the top surface of the replica. The top surface does not give any information other than showing that the surface is very shiny.

As Figure 4.17 shows, the underside of the replica showed in Figure 4.16 is also shiny. In Figure 4.18 the same replica is found to the left and 3 other replicas are showed next to it. In this case the focus is on the replicas, thus the lamp is out of focus.

These results seem to prove that whether a material is shiny or not, depends a lot of the surface structure. A glossy surface will reflect light like a mirror, which means that the direction of the reflected light is given by the direction of the incoming light. The law of reflection for mirrors state that the angle of incidence (the angle between the direction of the incoming light and the surface normal), is equal to the angle of reflection (the angle between the surface normal and the direction of the reflected light). A dim surface will reflect light in all directions. This can intuitively be related to rough and smooth surfaces, as a smooth surface has a constant surface normal, while a rough surface will

---

[3] Struers http://www.struers.com

Figure 4.16: The casting compound applied on a glass plate to. It should be noted that the light from a lamp in the ceiling is reflected on the surface of the glass plate. The focus is however on the casting material and not on the reflected image of the lamp.

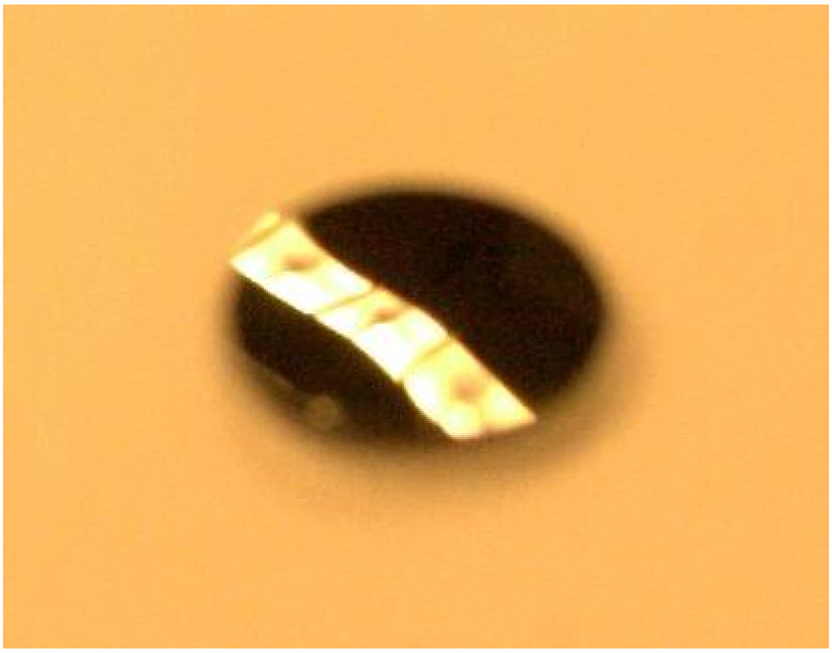

Figure 4.17: The surface of the glass plate is replicated and does indeed reflect light from the lamp in the ceiling. Here, the focus is on the image of the lamp, thus the replica is out of focus.

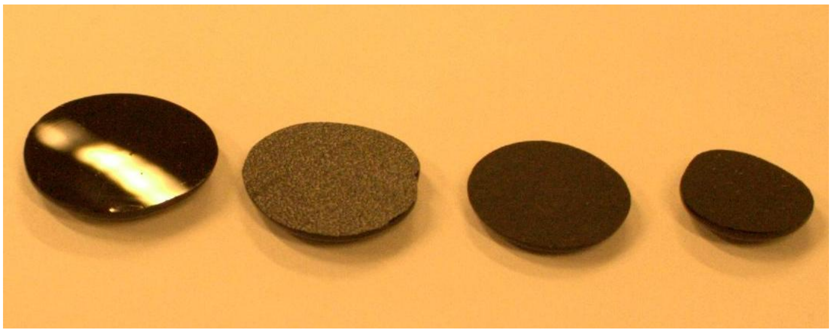

Figure 4.18: Replicas of 4 different surfaces. From the left: Glass plate, top of a metal computer cabinet, paperboard, ordinary paper. Note that, although the replica of the computer cabinet does not look as shiny as the glass replica, it does reflect more light in the direction of the camera than the two replicas to the right.

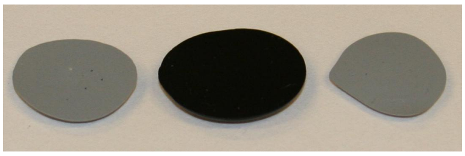

Figure 4.19: Three different replicas of rough surfaces. The middle replica is made using RepliSet F1 compound, while the two others are made using the grey RepliSet GF1 compound.

have variable surface normal, and will thus not reflect all the light in the same direction. A surface with roughness on a large length scale will still reflect more light in the direction given by the reflection law, but some of the light will be reflected in different directions. Surfaces with roughness on a shorter length scale will reflect light more evenly in all directions. To be able to analyse surfaces with laser profilometry, the surface has to be rough on very small length scales.

The fact that the replicas of the fracture surface is shiny, means that the fracture surface is shiny also, unless the casting process is affecting the surface structure. Direct observations do however confirm that the fracture surface is shiny. So even if the surface is difficult to measure using laser profilometry, the gloss gives some information about the surface structure.

4.4.2 Preliminary Laser Profilometry Analysis

The Laser Profilometry measurements were performed by Gary Chinga, researcher at the Paper and Fibre Research Institute (PFI). He offered to do some tests after it turned out that the people in Strasbourg were unable to obtain any results. Gary Chinga suggested to apply a method used for analysing paper, which involves that the surface is covered with a thin layer of gold to improve the light reflection properties. This was done and the test measurements were successful. A similar replica to the ones measured is shown in Figure 4.20

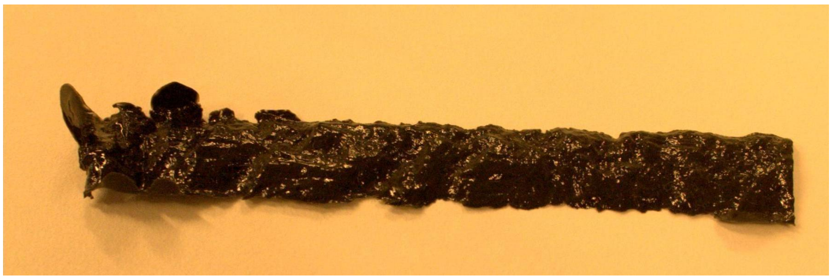

Figure 4.20: A replica similar to the replicas that were analysed with laser profilometry.

Both of the two types of casting material were analysed and both the grey (RepliSet GF1), and the black (RepliSet F1) proved to be suitable for this analysis. Figures 4.21 and 4.22 show the surface of two different replicas. Although it says “Gray Value” on the y-axis, it has been confirmed that the actual unit is μm on both axes. The profiles do not show roughness on large length scales, due to the band pass filtering, but this can easily be done in future measurements.

The replica of the news print surface shown in Figure 4.23 seems to be ok and have the roughness values typical for newsprint samples, according to Gary Chinga.

Although this looked promising for future analysis of fracture surfaces, there is a possibility that the casting process actually affects the fracture surface, causing it to change when in contact with the silicon rubber. First of all, the sample will

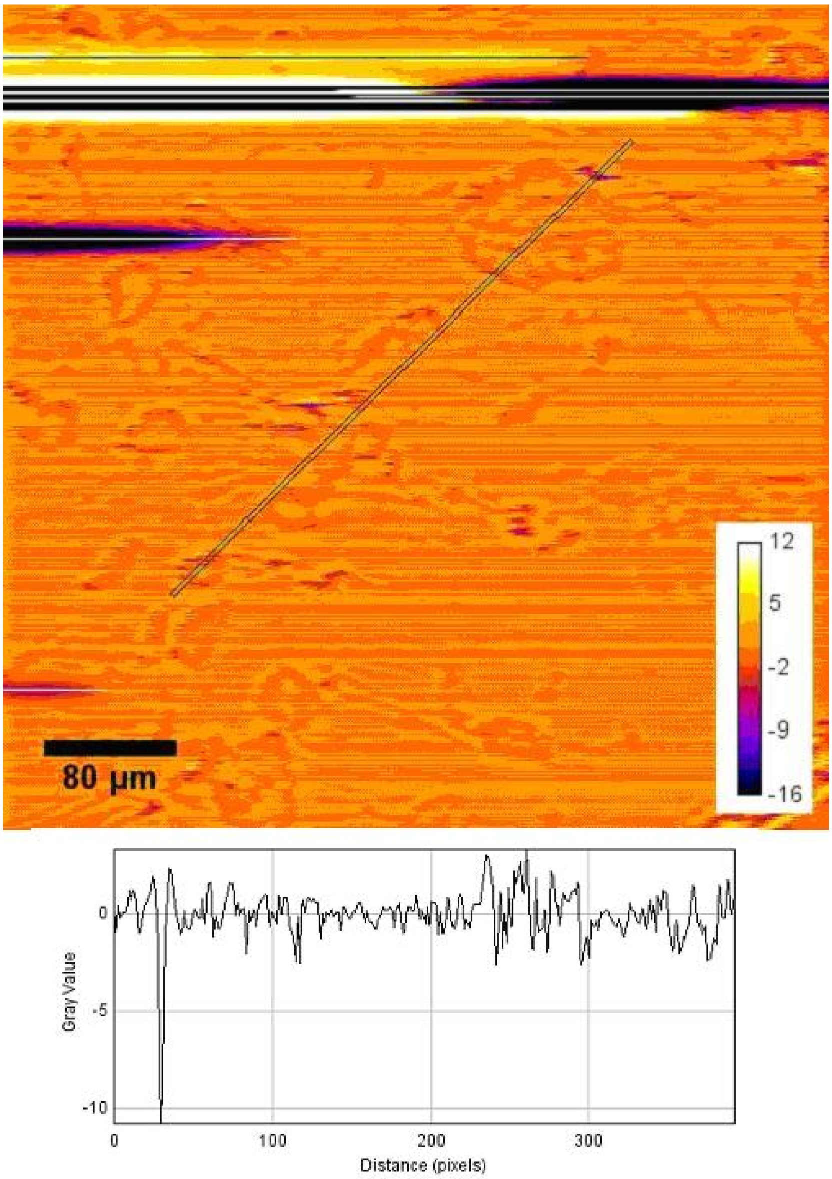

Figure 4.21: A square area of 0.5 mm × 0.5 mm of a replica made with RepliSet GF1, analysed with laser profilometry. The resolution is 1 pixel per μm. The surfaces were band-pass filtered to keep the structure between 1 and 10 μm and thus remove the curvature. The plot shows the surface profile at the indicated line. The units are μm on both the y-axis and the x-axis.

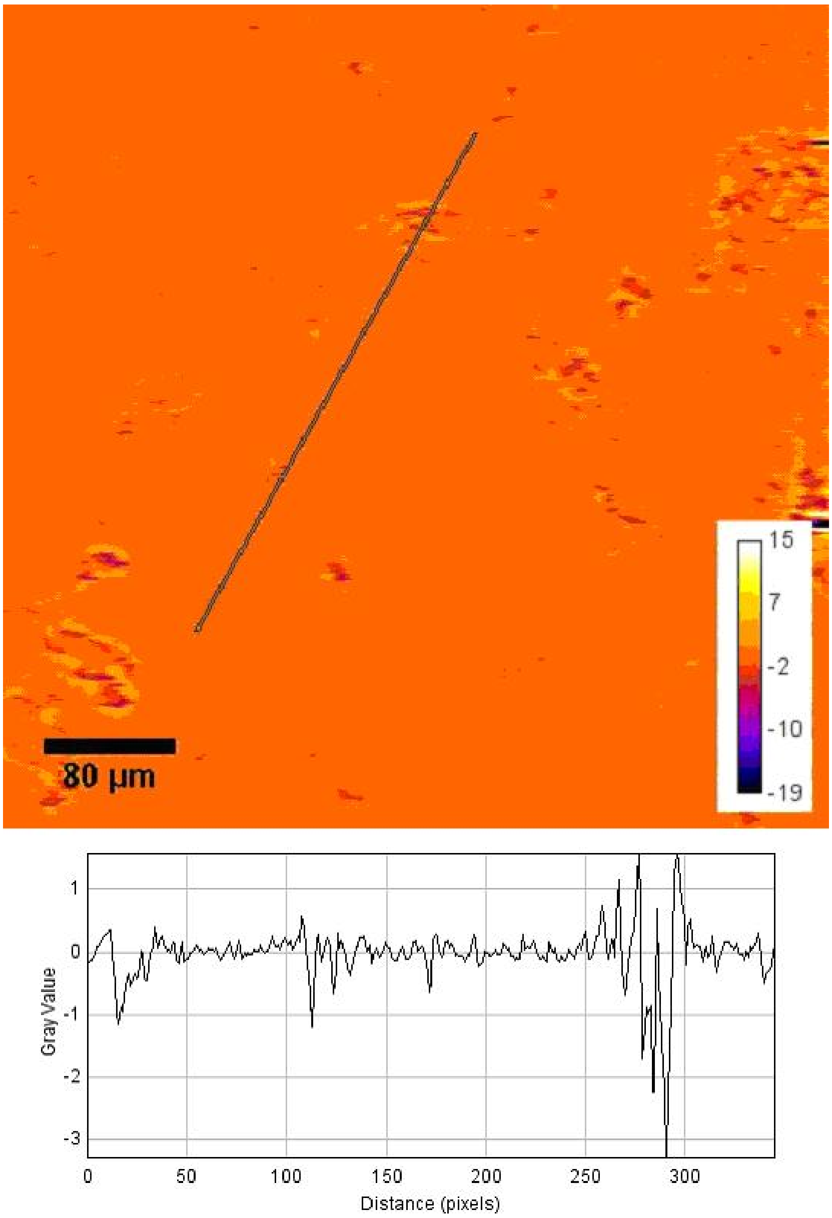

Figure 4.22: A square area of 0.5 mm × 0.5 mm of a replica made with RepliSet F1, analysed with laser profilometry. The resolution is 1 pixel per μm. The surfaces were band pass filtered to keep the structure between 1 and 10 μm and thus remove the curvature. The plot shows the surface profile at the indicated line. The units are μm on both the y-axis and the x-axis.

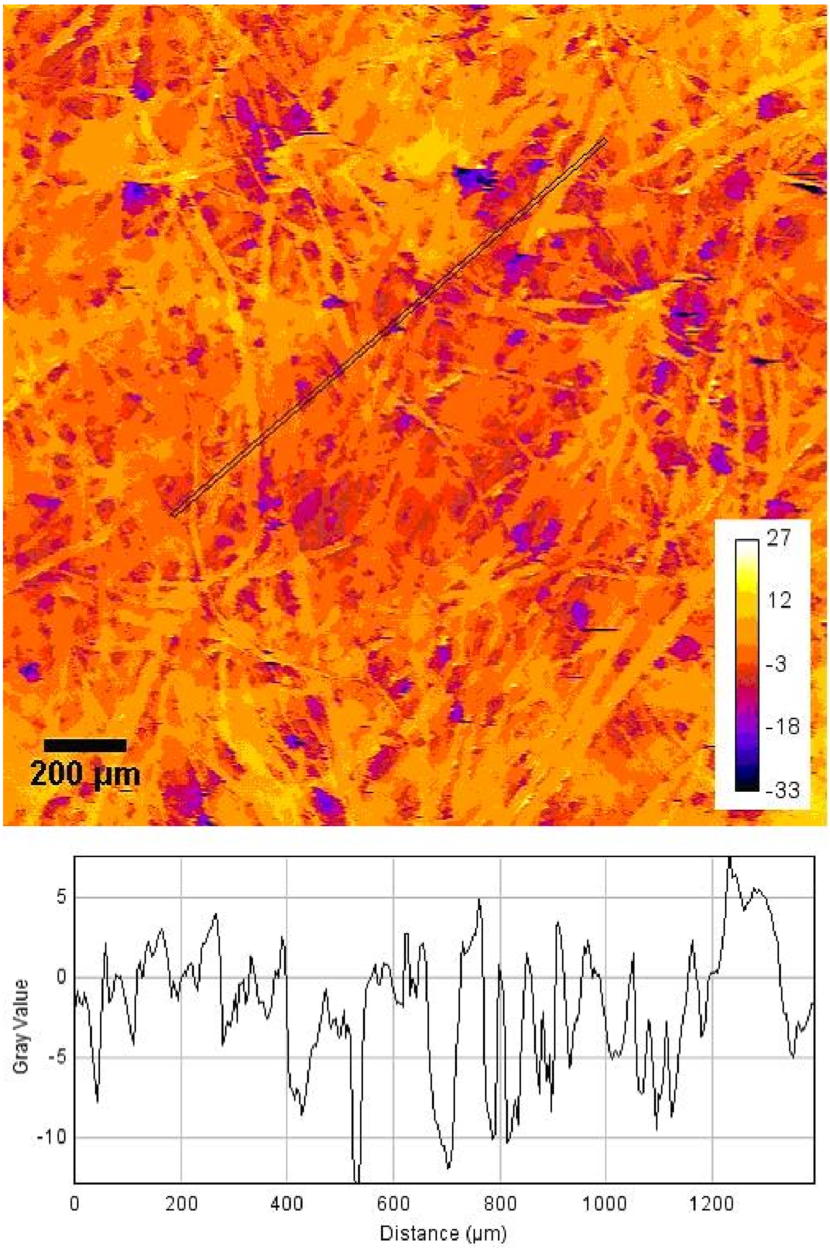

Figure 4.23: A square area of 2 mm × 2 mm of a news print sample replica. The plot shows the surface profile at the indicated line. The resolution is 1 pixel per 4 μm. The units are μm on both the y-axis and the x-axis.

be exposed to a certain pressure due gravity when the silicon rubber is applied on top of the surface. Secondly, the casting material is also a gel for about 30 seconds after it is applied on top of the surface, and there is a possibility that interactions between the gels, change the shape of the fracture surface. Henrik Hemmen has performed measurements on a larger length scale using magnetic resonance imaging (MRI) to measure the sample directly. This was done at the Federal University of Pernambuco (UFPE) in Recife, Brazil and a trip to Recife was also planned during my project in order to measure samples using MRI directly and also make castings of the same samples and measure them with laser profilometry. By comparing the two different methods, it should be possible to say something about the accuracy of the replicas, at least on a larger length scale, depending on the resolution of the MRI measurements which is approximately 0.1 mm. Unfortunately the MRI equipment was damaged shortly before I arrived in Recife, so the MRI analysis had to be cancelled. However I successfully made some samples and castings there in addition to testing some new equipment used for measuring the force.

4.4.3 Surface Analysis

As explained earlier, one of the main goals in this project is to analyse the fracture surfaces and calculate the roughness exponent. There are several different ways of estimating the roughness exponent. Henrik Hemmen [16], who analysed similar surfaces using MRI last year, made use of three different methods; the detrended fluctuation analysis, the Fourier transform of the height-height correlation function, and the second order correlation function. All of these methods are used in Appendix A, where the results are compared directly to those obtained by Henrik Hemmen. However, due to lack of time and computing power, only the detrended fluctuation analysis will be used for the laser profilometry data. As discussed by Bakke et. al. [17], the detrended fluctuation method seems to give quite adquate results for the values of ζ that was found with the resolution used, although it would be an advantage to compare the results with thos obtained with other methods.

Laser Profilometry Measurements

Measuring the castings using laser profilometer turned out to be quite difficult. First of all, the castings needed to be covered with gold before they could be measured. Secondly, the area measured could not exceed 5 mm × 5 mm because the laser profilometer can not handle too large variations of the height. First, some attempts to measure a square area of 10 mm × 10 mm were made. But all the attempts failed and the area had to be reduced to 5 mm × 5 mm. Measuring the smaller area, some of the measurements still failed, but eventually 9 samples were successfully measured. During this project, a lot more samples and castings were made, but because of the compliactions with measuring the castings, only 8 castings, prepared in Trondheim at NTNU, were analysed, in addition to 1 casting (numbered 9) made in Recife at the UFPE. The resolution of the measurements is 512 × 512 pixels, so the pixel size is just below 10 μm × 10 μm. The resolution of the pixel-values, i.e. the resolution in z-direction is on nanometer-scale, although the exact number has not been obtained. However, the accuracy is more than sufficient for this analysis. 3D plots of the measured areas are shown in Figures 4.24 to 4.32. The castings are numbered from 1 to 9 and information about each casting is given in Table 4.2.

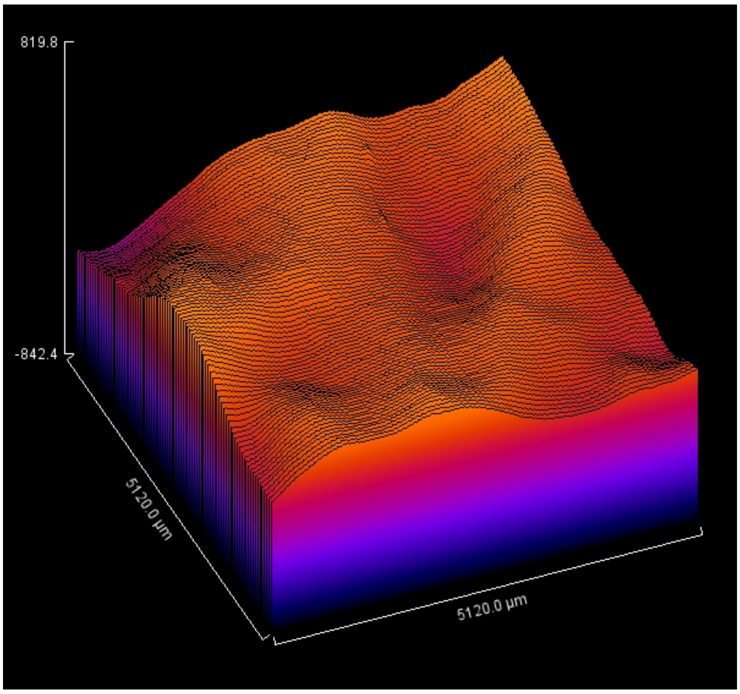

Figure 4.24: A square area of 5 mm × 5 mm of casting 1. The resolution is approximately 1 pixel per 10 μm.

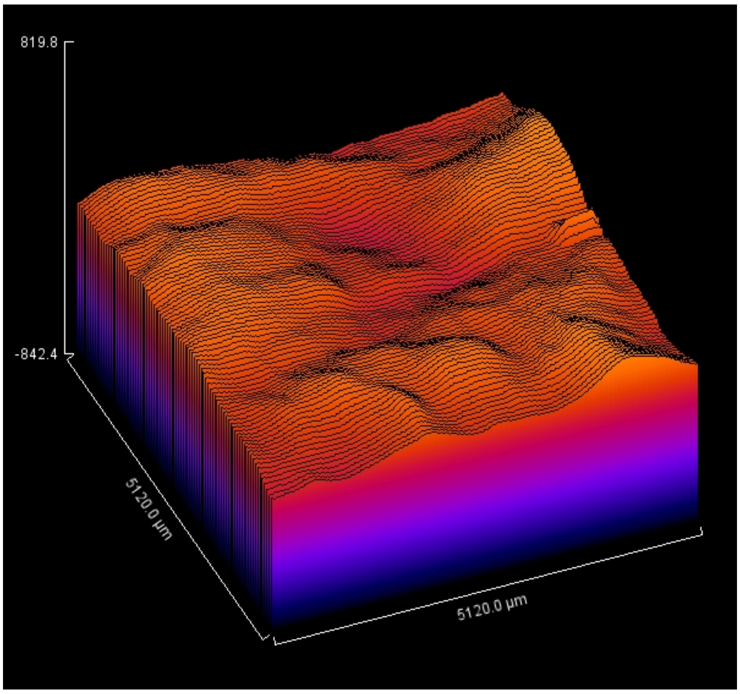

Figure 4.25: A square area of 5 mm × 5 mm of casting 2. The resolution is approximately 1 pixel per 10 μm.

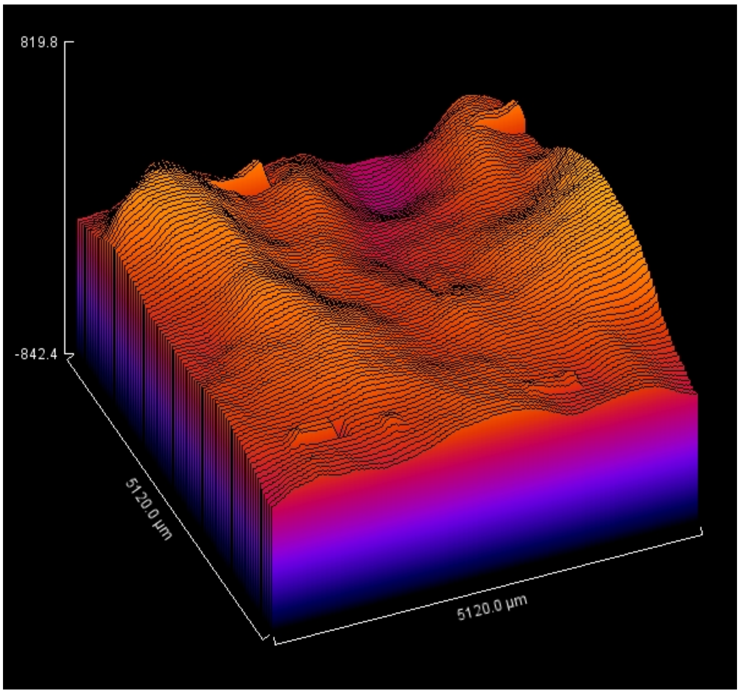

Figure 4.26: A square area of 5 mm × 5 mm of casting 3. The resolution is approximately 1 pixel per 10 μm.

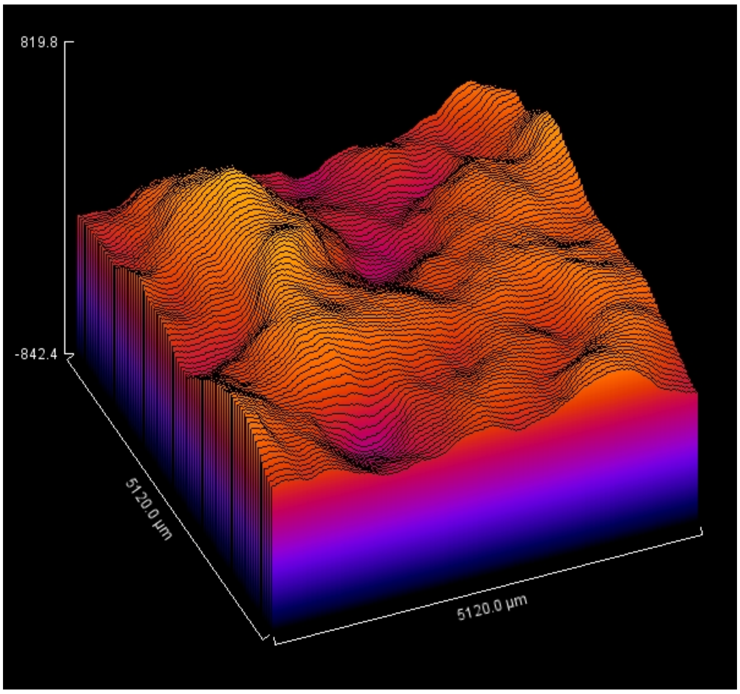

Figure 4.27: A square area of 5 mm × 5 mm of casting 4. The resolution is approximately 1 pixel per 10 μm.

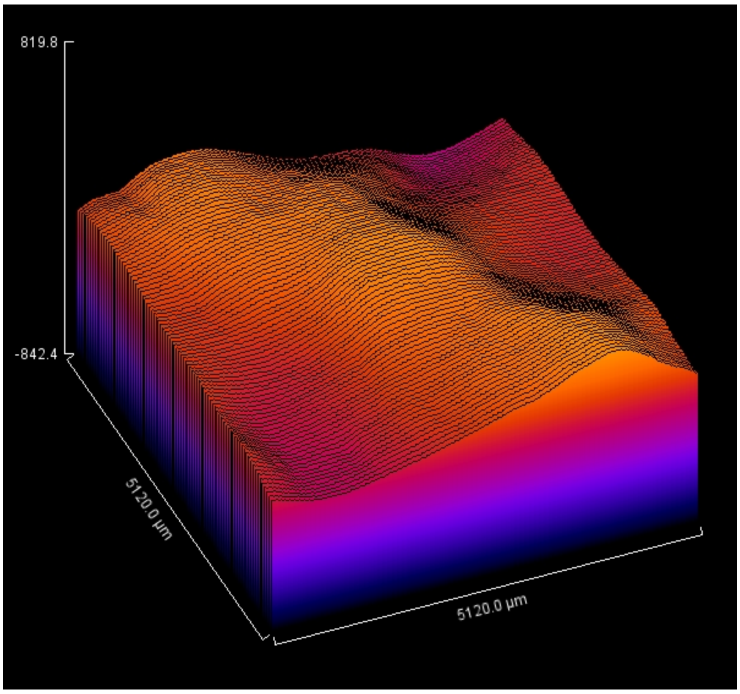

Figure 4.28: A square area of 5 mm × 5 mm of casting 5. The resolution is approximately 1 pixel per 10 μm.

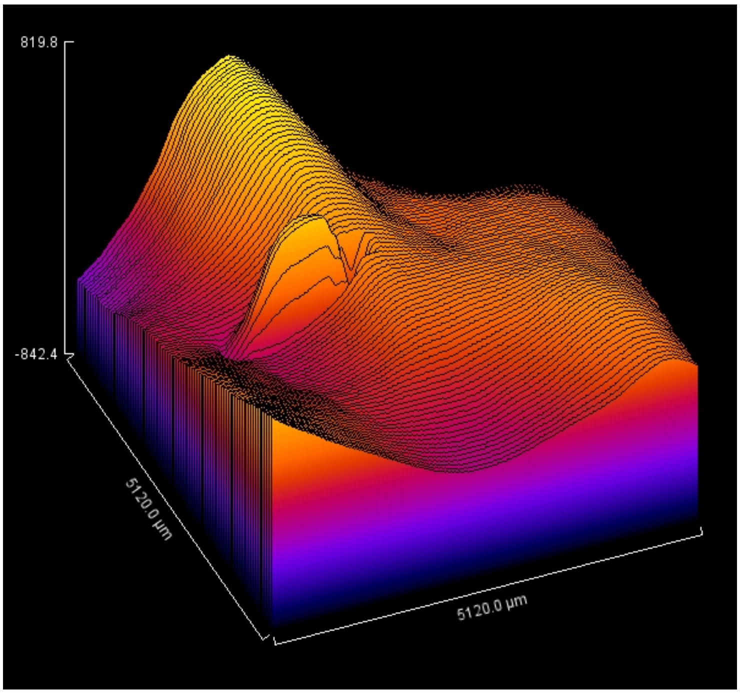

Figure 4.29: A square area of 5 mm × 5 mm of casting 6. The resolution is approximately 1 pixel per 10 μm.

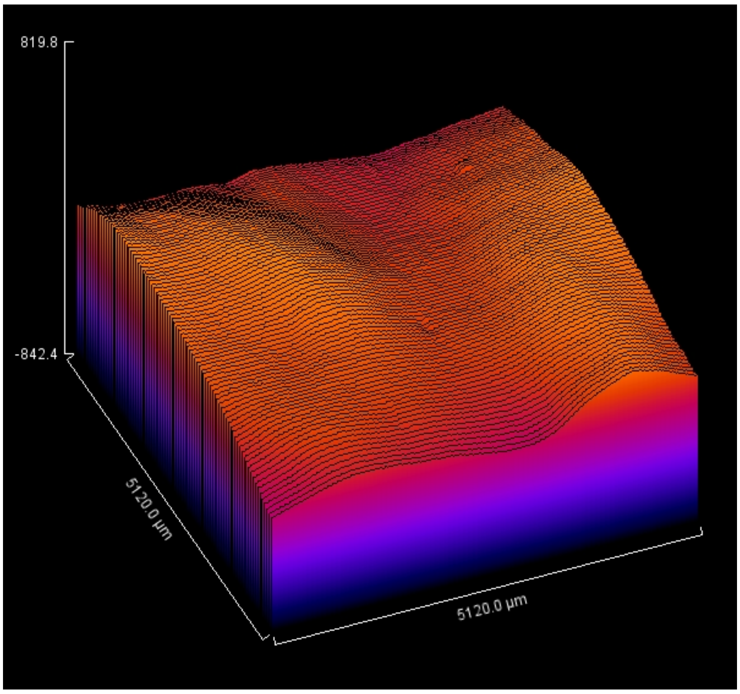

Figure 4.30: A square area of 5 mm × 5 mm of casting 7. The resolution is approximately 1 pixel per 10 μm.

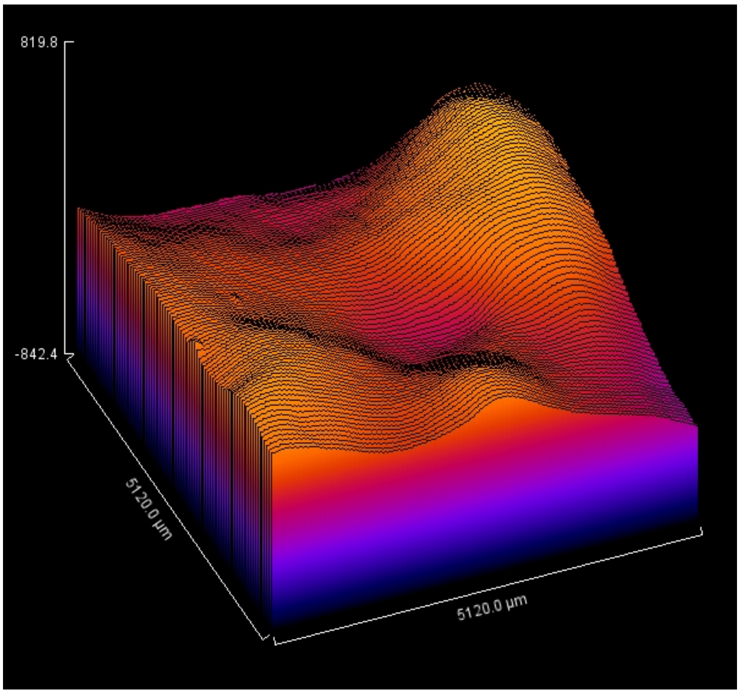

Figure 4.31: A square area of 5 mm × 5 mm of casting 8. The resolution is approximately 1 pixel per 10 μm.

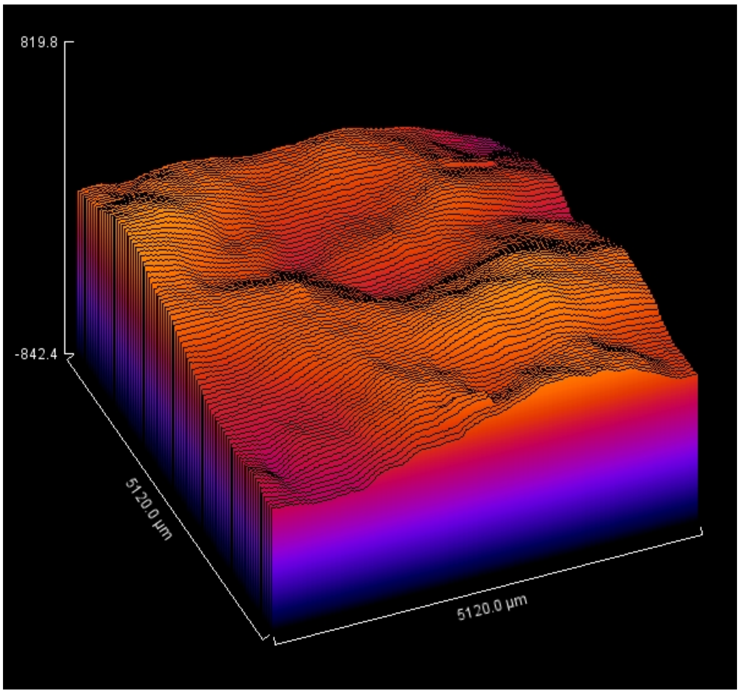

Figure 4.32: A square area of 5 mm × 5 mm of casting 9. The resolution is approximately 1 pixel per 10 μm.

It should be mentioned that sample number 9, which was made in Recife at the UFPE, was not filtered. Since unfiltered samples sets into a gel much quicker than filtered samples, the experiment was performed after only 3 days. The rest of the samples, numbered 1 to 8, were filtered samples.

Table 4.2: Descripition of each sample used to make the castings measured with Laser Profilometry.

Sample number #	v_p (mm/s)	v_f (mm/s)	Sample age (days)
1	0.05	0.0354	11
2	0.1	0.0707	7
3	0.2	0.1414	9
4	0.3	0.2121	11
5	0.4	0.2828	10
6	0.5	0.3536	10
7	0.7	0.4950	10
8	0.9	0.6364	10
9	0.4	0.2828	3

The fracture velocity v_f is given by (4.16) and it was the positioner velocity v_p that was given as input to the positioner.

Roughness Exponent Calculations

The roughness exponent ζ was calculated using the detrended fluctuation method. As discussed by Bakke et. al.[17], the detrended fluctuation method seems to give quite accurate results for a profile size of 512 datapoints and a true roughness exponent of $\zeta = 0.8$.

A Matlab script was written to analyse the data. The first part of the script imported the data from an ascii-file and stored it in a 2-dimensional Matlab variable. Then the function $\omega(\Delta)$ was calculated. The data points for each Δ was calculated for all slices and then averaged over all slices. The data was then stored to a file. Finally ω was plotted against Δ in a loglog-plot and a straight line was plotted to match the linear part of the plot. The slope of this straight line is the roughness exponent ζ, as shown in (4.23). This can easily be shown as (2.4) gives

$$\omega = c_1 \Delta^{\zeta} \tag{4.22}$$

for some constant c_1. Taking the logarithm on boths sides of(4.22) gives

$$\log \omega = \log c_1 + \zeta \log \Delta \tag{4.23}$$

and the slope is ζ.

The Matlab code that calculates the function $\omega(\Delta)$ is shown in Figure 4.33.

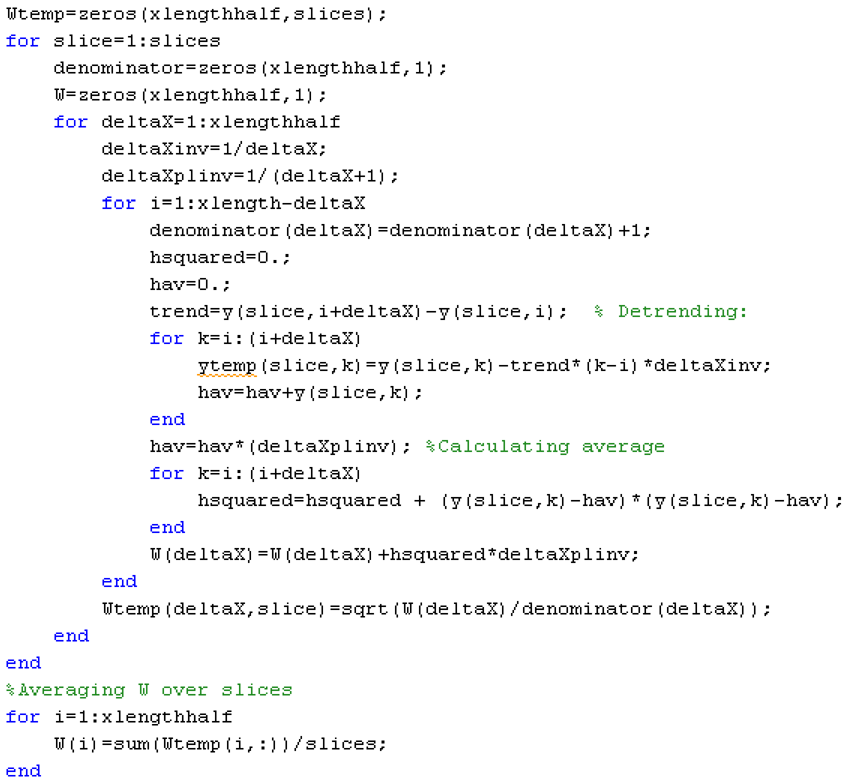

```
Wtemp=zeros(xlengthhalf,slices);
for slice=1:slices
    denominator=zeros(xlengthhalf,1);
    W=zeros(xlengthhalf,1);
    for deltaX=1:xlengthhalf
        deltaXinv=1/deltaX;
        deltaXplinv=1/(deltaX+1);
        for i=1:xlength-deltaX
            denominator(deltaX)=denominator(deltaX)+1;
            hsquared=0.;
            hav=0.;
            trend=y(slice,i+deltaX)-y(slice,i);  % Detrending:
            for k=i:(i+deltaX)
                ytemp(slice,k)=y(slice,k)-trend*(k-i)*deltaXinv;
                hav=hav+y(slice,k);
            end
            hav=hav*(deltaXplinv); %Calculating average
            for k=i:(i+deltaX)
                hsquared=hsquared + (y(slice,k)-hav)*(y(slice,k)-hav);
            end
            W(deltaX)=W(deltaX)+hsquared*deltaXplinv;
        end
        Wtemp(deltaX,slice)=sqrt(W(deltaX)/denominator(deltaX));
    end
end
%Averaging W over slices
for i=1:xlengthhalf
    W(i)=sum(Wtemp(i,:))/slices;
end
```

Figure 4.33: Matlab code that calculates ω for each value of δ

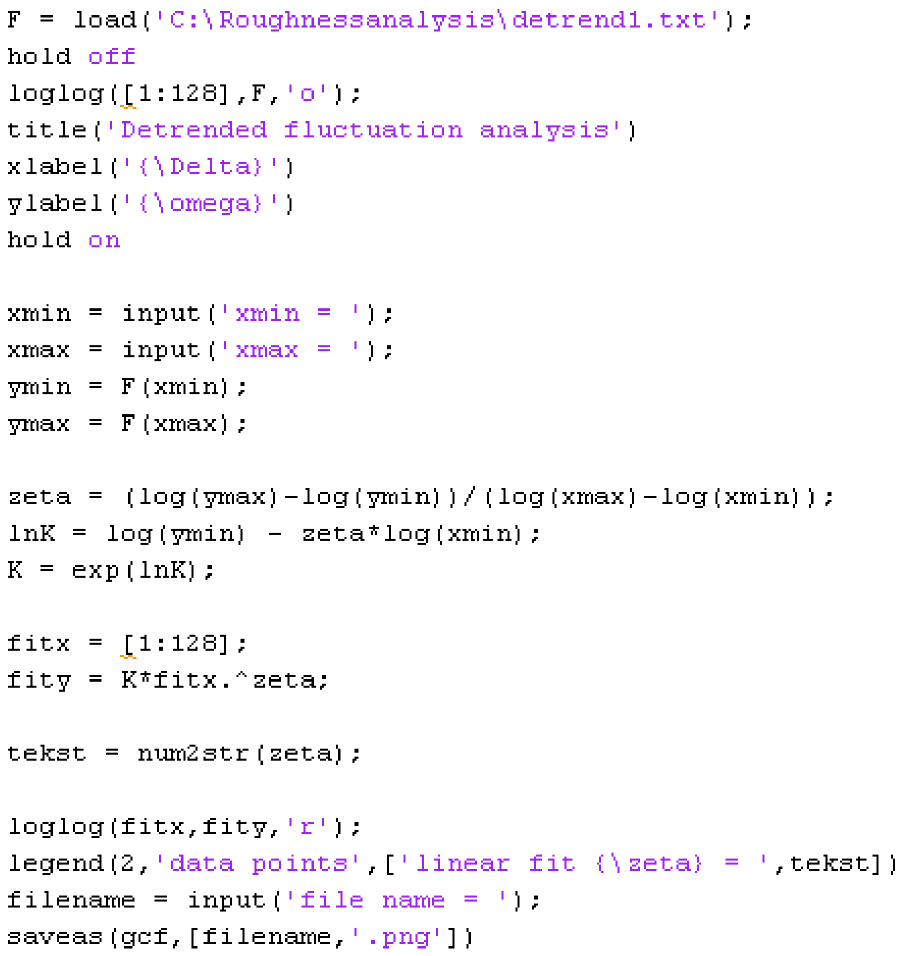

```
F = load('C:\Roughnessanalysis\detrend1.txt');
hold off
loglog([1:128],F,'o');
title('Detrended fluctuation analysis')
xlabel('{\Delta}')
ylabel('{\omega}')
hold on

xmin = input('xmin = ');
xmax = input('xmax = ');
ymin = F(xmin);
ymax = F(xmax);

zeta = (log(ymax)-log(ymin))/(log(xmax)-log(xmin));
lnK = log(ymin) - zeta*log(xmin);
K = exp(lnK);

fitx = [1:128];
fity = K*fitx.^zeta;

tekst = num2str(zeta);

loglog(fitx,fity,'r');
legend(2,'data points',['linear fit {\zeta} = ',tekst])
filename = input('file name = ');
saveas(gcf,[filename,'.png'])
```

Figure 4.34: Matlab code that plots the function and the linear fit. It also writes the calculate value of ζ.

To plot the function and the linear fit the Matlab code shown in Figure 4.34 was used:

The results of the analysis along the x-axis[4] are given in Figures 4.35 to 4.43.

The results of the analysis along the y-axis are given in Figures 4.44 to 4.52. The roughness exponents for all the samples are given in Table 4.3.

---

[4] The x-direction is the direction in which the fracture has propagated and must not be confused with the horizontal axis in the plots.

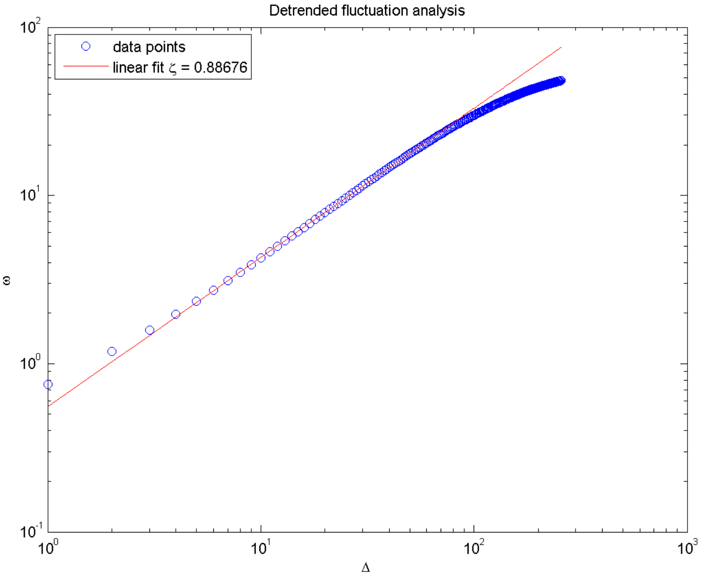

Figure 4.35: Detrended fluctuation analysis along the x-direction of sample 1, averaged over the y-direction. The unit along the horizontal axis in the plot is 10 μm.

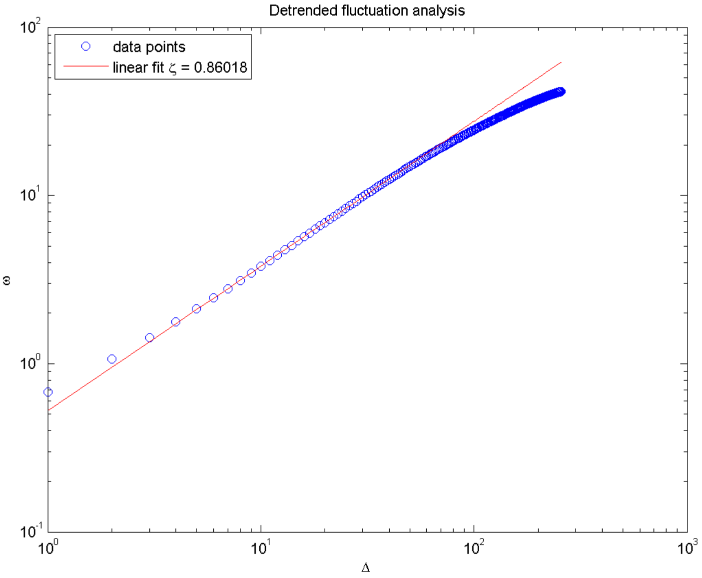

Figure 4.36: Detrended fluctuation analysis along the x-direction of sample 2, averaged over the y-direction. The unit along the horizontal axis in the plot is 10 μm.

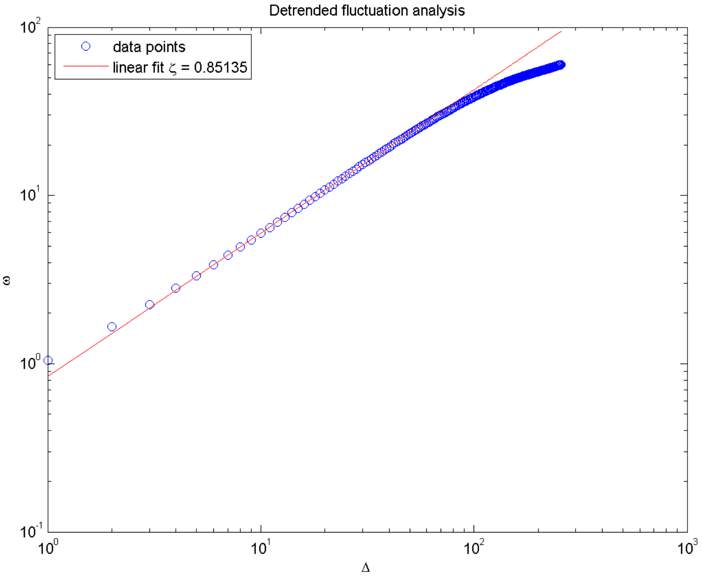

Figure 4.37: Detrended fluctuation analysis along the x-direction of sample 3, averaged over the y-direction. The unit along the horizontal axis in the plot is 10 μm.

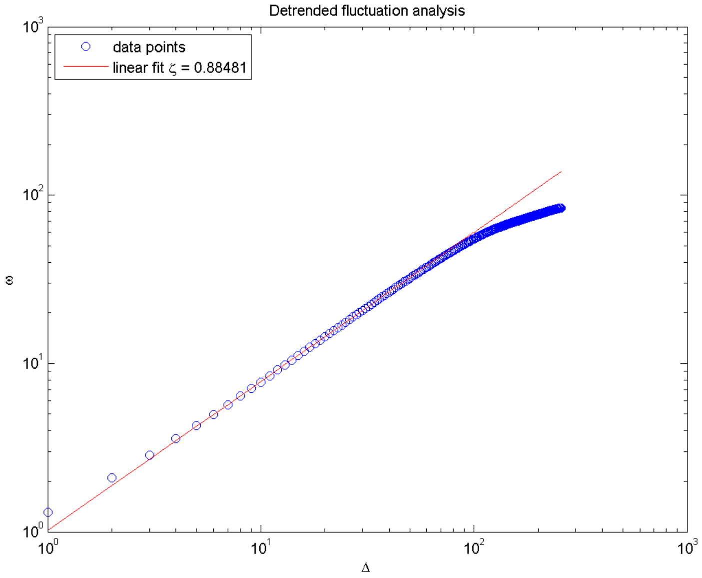

Figure 4.38: Detrended fluctuation analysis along the x-direction of sample 4, averaged over the y-direction. The unit along the horizontal axis in the plot is 10 μm.

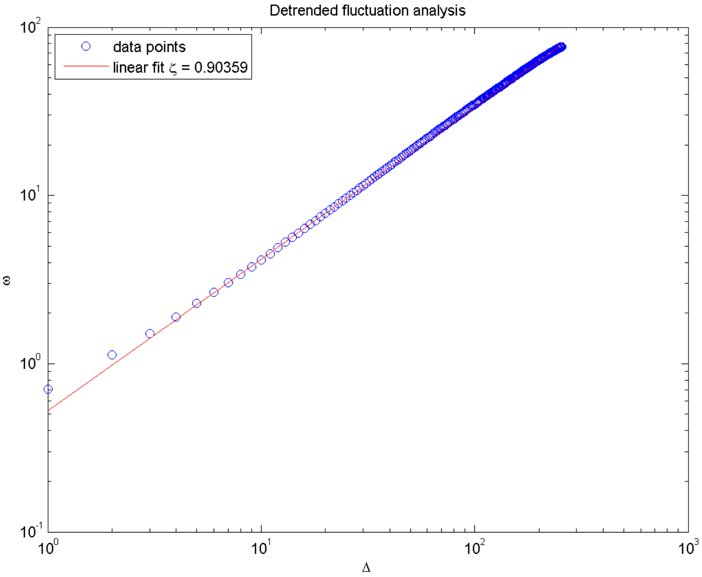

Figure 4.39: Detrended fluctuation analysis along the x-direction of sample 5, averaged over the y-direction. The unit along the horizontal axis in the plot is 10 μm.

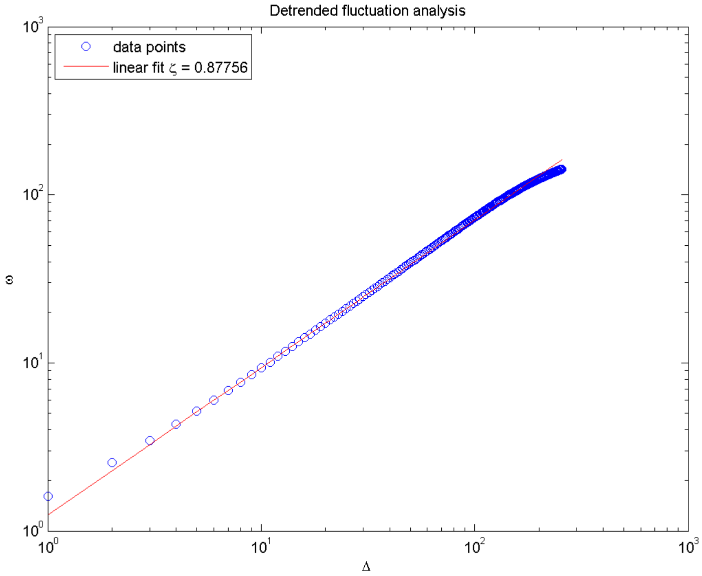

Figure 4.40: Detrended fluctuation analysis along the x-direction of sample 6, averaged over the y-direction. The unit along the horizontal axis in the plot is 10 μm.

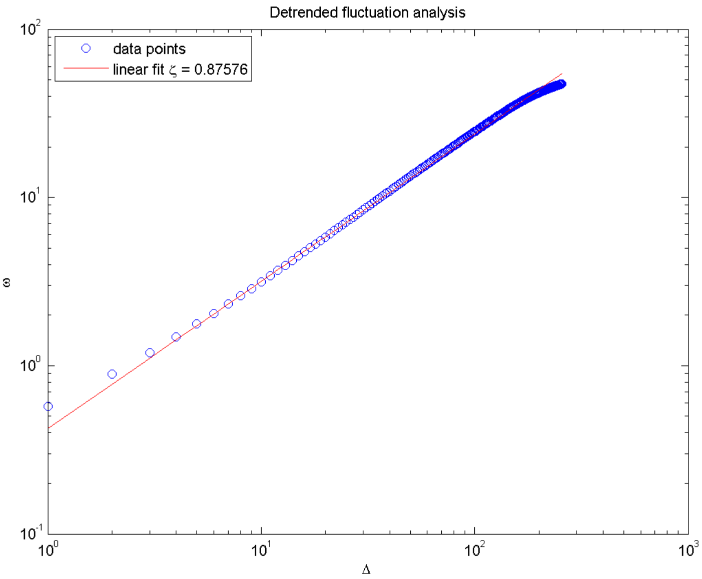

Figure 4.41: Detrended fluctuation analysis along the x-direction of sample 7, averaged over the y-direction. The unit along the horizontal axis in the plot is 10 μm.

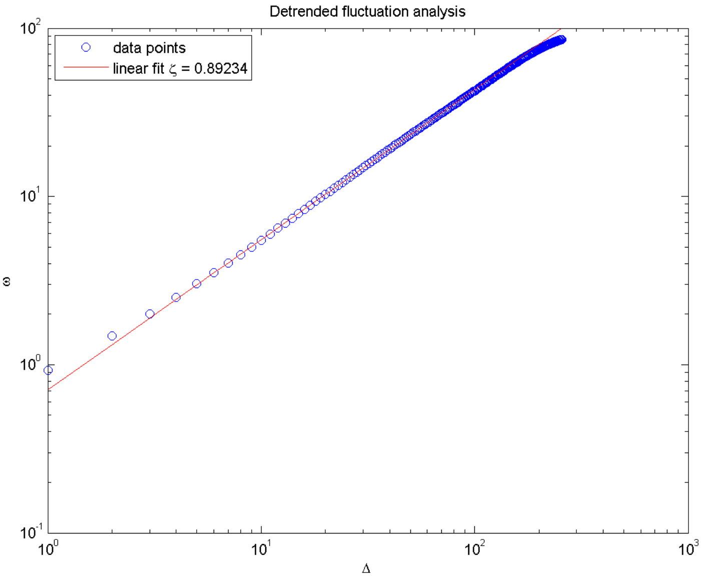

Figure 4.42: Detrended fluctuation analysis along the x-direction of sample 8, averaged over the y-direction. The unit along the horizontal axis in the plot is 10 μm.

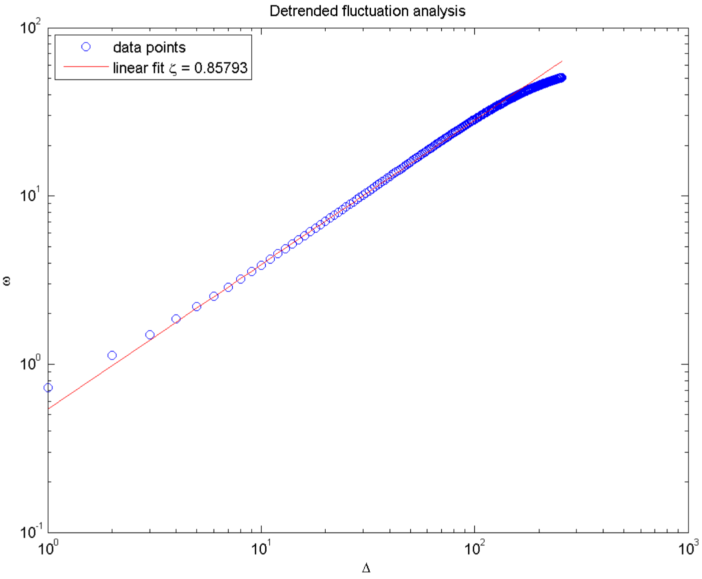

Figure 4.43: Detrended fluctuation analysis along the x-direction of sample 9, averaged over the y-direction. The unit along the horizontal axis in the plot is 10 μm.

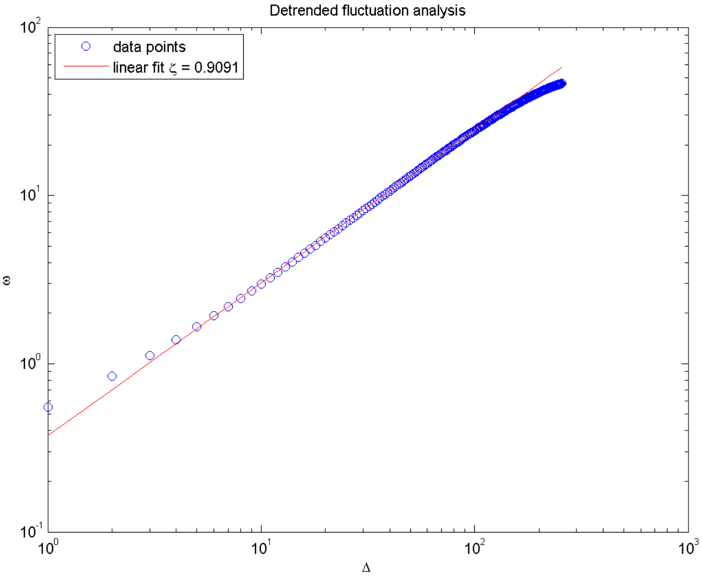

Figure 4.44: Detrended fluctuation analysis along the y-direction of sample 1, averaged over the y-direction. The unit along the horizontal axis in the plot is 10 μm.

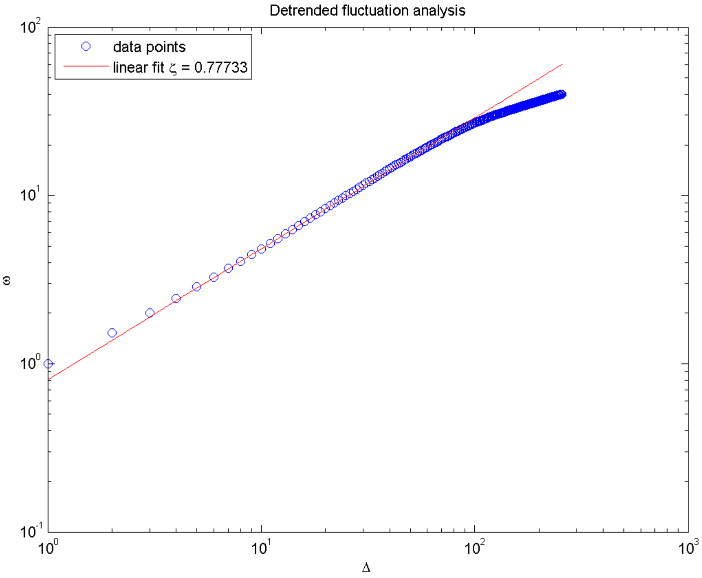

Figure 4.45: Detrended fluctuation analysis along the y-direction of sample 2, averaged over the y-direction. The unit along the horizontal axis in the plot is 10 μm.

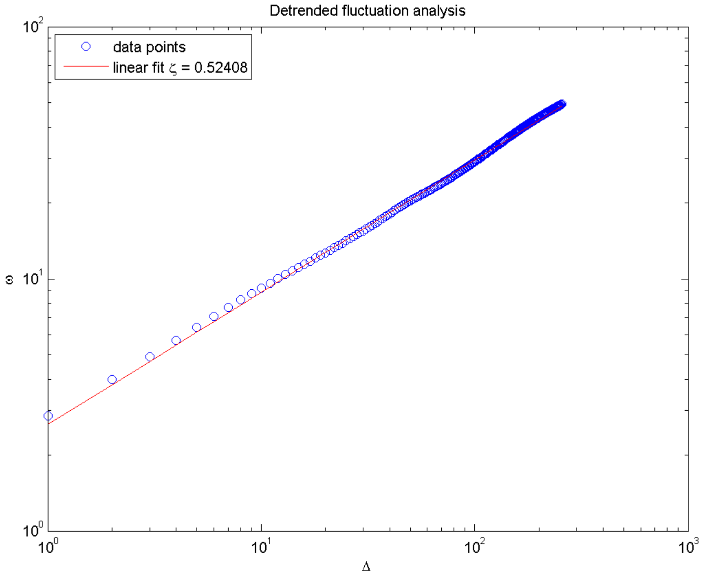

Figure 4.46: Detrended fluctuation analysis along the y-direction of sample 3, averaged over the y-direction. The unit along the horizontal axis in the plot is 10 μm.

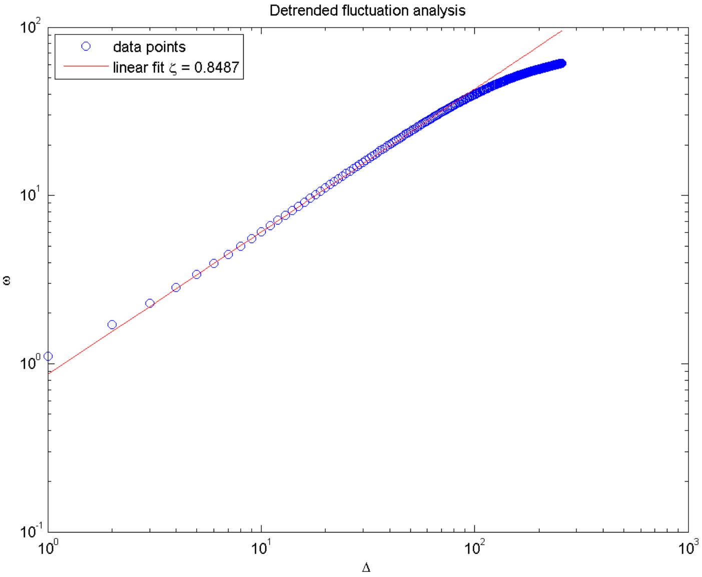

Figure 4.47: Detrended fluctuation analysis along the y-direction of sample 4, averaged over the y-direction. The unit along the horizontal axis in the plot is 10 μm.

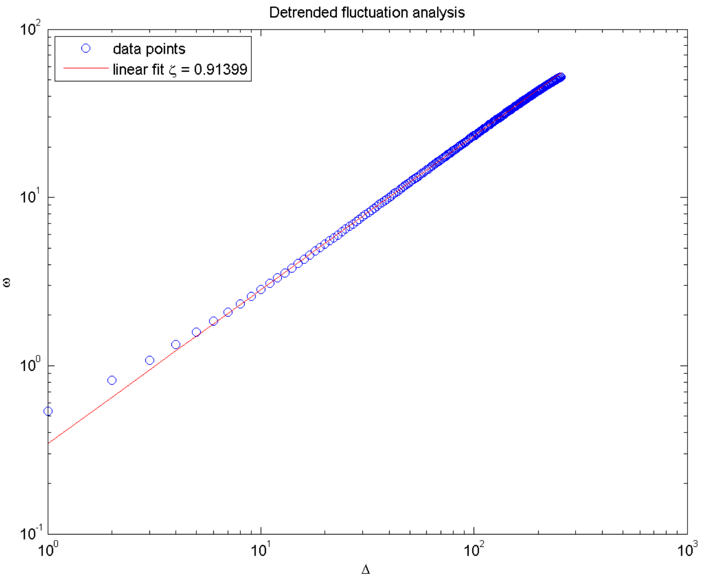

Figure 4.48: Detrended fluctuation analysis along the y-direction of sample 5, averaged over the y-direction. The unit along the horizontal axis in the plot is 10 μm.

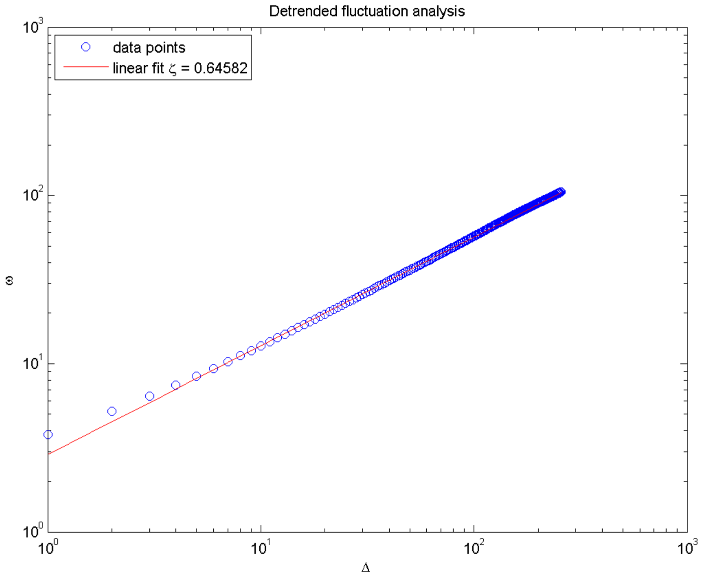

Figure 4.49: Detrended fluctuation analysis along the y-direction of sample 6, averaged over the y-direction. The unit along the horizontal axis in the plot is 10 μm.

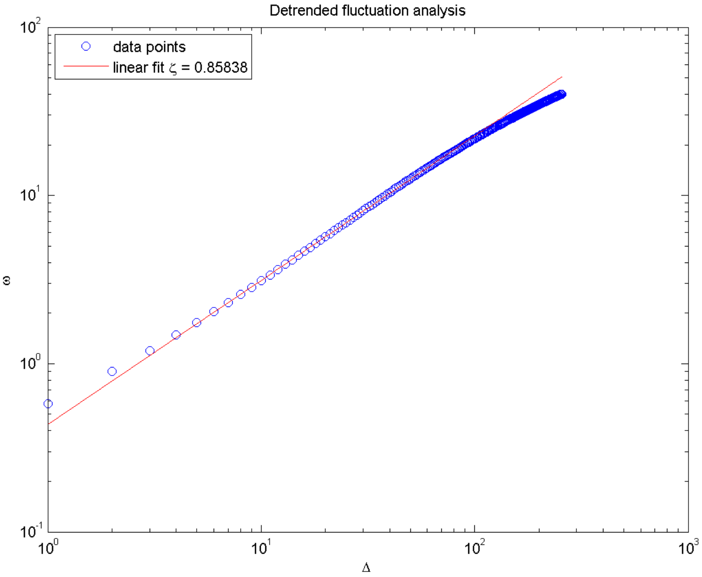

Figure 4.50: Detrended fluctuation analysis along the y-direction of sample 7, averaged over the y-direction. The unit along the horizontal axis in the plot is 10 μm.

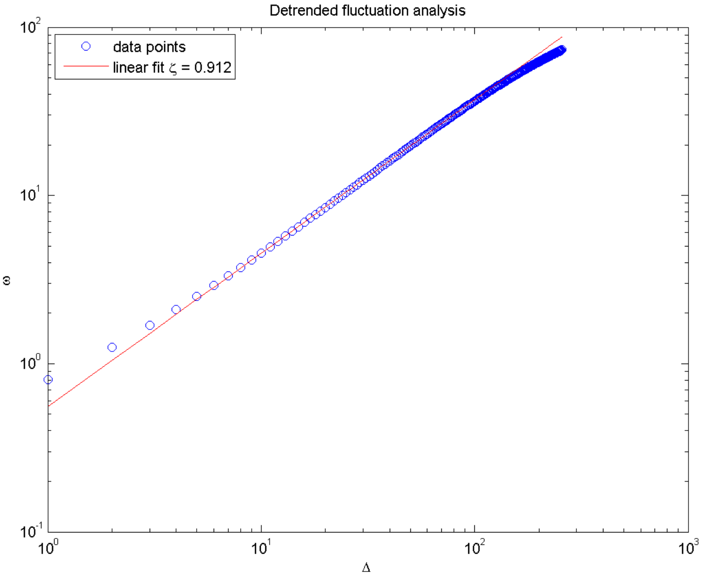

Figure 4.51: Detrended fluctuation analysis along the y-direction of sample 8, averaged over the y-direction. The unit along the horizontal axis in the plot is 10 μm.

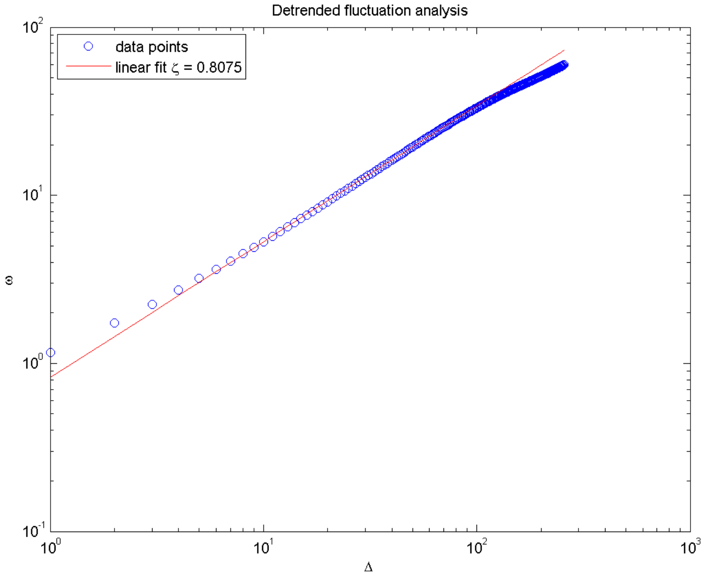

Figure 4.52: Detrended fluctuation analysis along the y-direction of sample 9, averaged over the y-direction. The unit along the horizontal axis in the plot is 10 μm.

Table 4.3: The calculated roughness exponents for each sample.

Sample number	ζ in x-direction	ζ in y-direction
1	0.89	0.91
2	0.86	0.78
3	0.85	0.52
4	0.88	0.85
5	0.90	0.91
6	0.88	0.65
7	0.88	0.86
8	0.89	0.91
9	0.86	0.81

It is worth noticing that the roughness exponent in the direction in which the fracture has propagated is almost the same for all samples, while the roughness exponent in the direction perpendicular to that of the fracture propagation is varying a lot more. The results obtained here are of course exposed to unsystematic errors because only one sample for each velocity was measured and each sample has only been measured once. But the fact that the roughness exponent in x-direction is more or less the same, can indicate that such errors has not affected the experimental part considerably. From the data obtained here, there is no apparent correlation between the fracture propagation velocity and the roughness of the surface.

Chapter 5

Concluding Remarks

The work in this project was based on the experimental setup designed by Christian A. Nielsen [1] which in turn was adapted from the peel-test like method applied by Tanaka et. al. [3]. The setup has been successfully improved in certain aspects in order to find a way to investigate the fracture surfaces and the fracture fronts. The method used for finding the fracture energy has been evaluated, but the main focus has been elsewhere and no improvements have been made or suggested.

The main goal was to investigate if there is a dependence between the roughness of the fracture surface and the fracture propagation velocity. No such dependence was found.

Suggestions for future studies

One important test that needs to be done in the future, to validate the results obtained in this project, is to do measurements on the samples themselves, for instance using MRI. It is not known whether the casting procedure changes the surface of the sample, so one should measure the sample with MRI and then make a casting of the same sample and measure it with laser profilometry. Then the results can be compared. Not necessarily the roughness exponent, but the profile of the fracture surface.

To study the roughness of the fracture front using the method suggested here, the samples should be made considerably wider in order to allow a wider range of length scales studied.

Another interesting thing to study in the future could be the possible correlation between the age of the samples and the roughness of the fracture surface.

In general I would say that obtaining more definite results requires more resources than has been available for this project. More samples should be casted and measured with laser profilometry in order to provide a better statistical basis for analysis and limit unsystematic errors. The process of analysing the castings with laser profilometry is however quite complicated and the people in Strasbourg were not able to do it.

Bibliography

[1] Christian A. Nielsen. An experimental study of fractures in gels. Master's thesis, The Norwegian University of Science and Technology, 2007.

[2] Jon Otto Fossum. Complex physical phenomena in clays. *A. T. Skjeltorp & S. F. Edwards (eds.), Soft Condensed Matter: Configurations, Dynamics and Functionality*, 2000.

[3] Y. Tanaka, K. Fukao, and Y. Miyamoto. Fracture energy of gels. *The European Physics Journal E*, 3 (4), 2000.

[4] A. Mourchid, E. Lecolier, H. Van Damme, and P. Levitz. On viscoelastic, birefringent, and swelling properties of laponite clay suspensions: Revisited phase diagram. *Langmuir*, 14, 1998.

[5] Herman Z. Cummins. Liquid, glass, gel: The phases of colloidal laponite. *Journal of Non-Crystalline Solids*, 353, 2007.

[6] Jon Otto Fossum. Physical phenomena in clays. *Physica A*, 270, 1999.

[7] A. T. Zehnder. Lecture notes on fracture mechanics. `http://dspace.library.cornell.edu/handle/1813/3075`, Cornell University, Ithaca, New York, 2006.

[8] Y. Tanaka, K. Fukao, Y. Miyamoto, and K. Sekimoto. Discontinous crack fronts of three-dimensional fractures. *Europhysics Letters*, 43 (6), 1998.

[9] Jean-Pierre Vilotte Jean Schmittbuhl and Stéphane Roux. Reliability of self-affine measurements. *Physicala Review E*, 51, 1994.

[10] J. Feder. *Fractals*. Plenum, New York, 1988.

[11] F. Cousin, V. Cabuil, and P. Levitz. Magnetic colloidal particles as probes for the determination of the structure of laponite suspensions. *Langmuir*, 18, 2002.

[12] Micos GmbH. Product details. `http://www.micos.ws/`, 2006.

[13] HBM. Pw4krc3 data sheet. `http://www.hbm.com/`, 2007.

[14] E. Bouchaud, J.P. Bouchaud, D.S. Fisher, S. Ramanathan, and J.R. Rice. Can crack front waves explain the roughness of cracks? *Journal of the Mechanics and Physics of Solids*, 50, 2001.

[15] P. Daguier, B. Nghiem, E. Bouchaud, and F. Creuzet. Pinning and depinning of crack fronts in heterogeneous materials. *Physical Review Letters*, 78, 1996.

[16] Henrik Hemmen. Experimental studies of nano-structured clay gels. Master's thesis, The Norwegian University of Science and Technology, 2008.

[17] Jan Øystein Haavig Bakke and Alex Hansen. Accuracy of roughness exponent measurement methods. *Physical Review E*, 76, 2007.

Appendix A

Roughness Test Analysis

As part of his master's thesis, Henrik Hemmen [16] studied the same kind of Laponite gels in Recife using MRI to measure the fracture surfaces directly. In an attempt to verify the validity and accuracy of his measurements, he borrowed a silicone sample from Professor Jean Schmittbuhl in Strasbourg and measured it using MRI. Professor Schmittbuhl measured the same sample with laser profilometry and the idea was to compare the results from these two different methods. But apparently there were some sort of confusion as to whether the data initially sent by Professor Schmittbuhl was correct. This was discovered some time afterwards and Professor Schmittbuhl measured the sample again and sent the data. However, Professor Schmittbuhl did not finish the measurements in time for Henrik Hemmen to include them in his thesis. For that reason I was asked to analyse the data sent from Professor Schmittbuhl and calculate the roughness exponent using the same methods as Henrik Hemmen used.

A.1 Roughness of Silicon Sample

The roughness exponent was calculated using three different methods: The second order correlation function, the Fourier transform of the height-height correlation function and the detrended fluctuation analysis which has been described and used earlier in this report. The other two methods; the second order correlation function (A.1), and the Fourier transform of the height-height correlation function (A.2) and (A.3), are described below.

$$C_2(r) = \Big\langle \big(h(x+r) - h(x)\big)^2 \Big\rangle_x^{1/2} \propto r^{\zeta} \tag{A.1}$$

Here, $h(x)$ is a height profile in one dimension. The third method involves calculating the height-height correlation function:

$$C(r) = \big\langle \big(h(x) - \bar{h}\big)\big(h(x+r) - \bar{h}\big) \big\rangle \tag{A.2}$$

and then take the Fourier transform. Now, the power spectrum $S(\omega)$ of C scales as:

$$S(\omega) \propto \omega^{-(1+2\zeta)} \tag{A.3}$$

As with the detrended fluctuation analysis, the roughness exponent is found by fiting a straight line to the loglog-plot of the power law function. In the case of the Fourier transform of the height-height correlation function, the slope k of the linear fit is not ζ itself, but $-(1+2\zeta)$. This means that the roughness exponent is given by (A.4).

$$\zeta = -\frac{k+1}{2} \tag{A.4}$$

As before, to keep track of the directions, the direction in which the fracture has propagated will be refered to as the x-axis, while the direction across the sample perpendicular to the direction in which the fracture has propagated will be refered to as the y-axis. The height of the fracture surface, above a smooth reference plane, is then the z-value. The measurements made by Professor Schmittbuhl has a resolution of 1999 × 2000 pixels and one pixel corresponds to 25 μm × 25 μm.

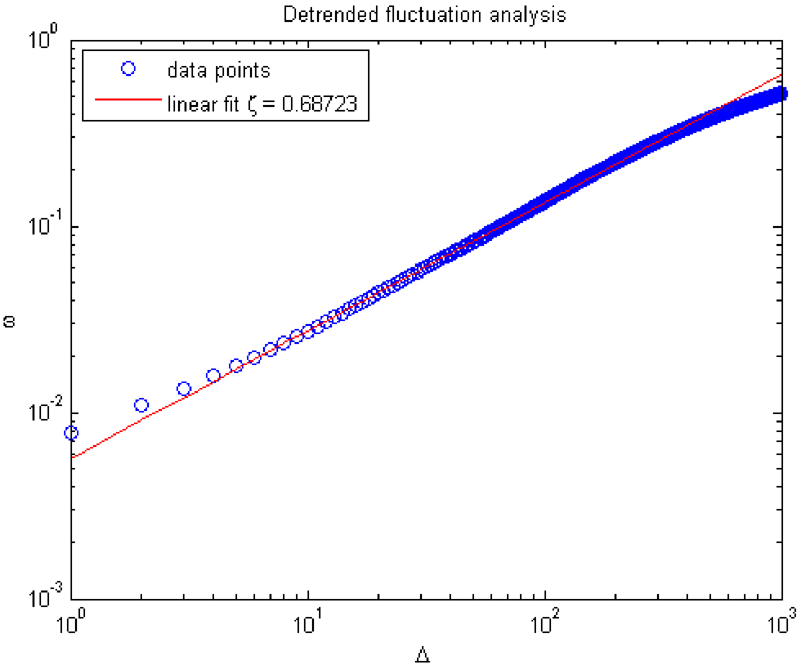

Figure A.1: Detrended fluctuation analysis calculated along the x-axis. ζ is the slope of the red line. The unit along the x-axis is pixels, i.e. the bandwith Δ in number of pixels. The pixel size is 25 μ m × 25 μ m, so the unit along the x-axis is 25 μ m.

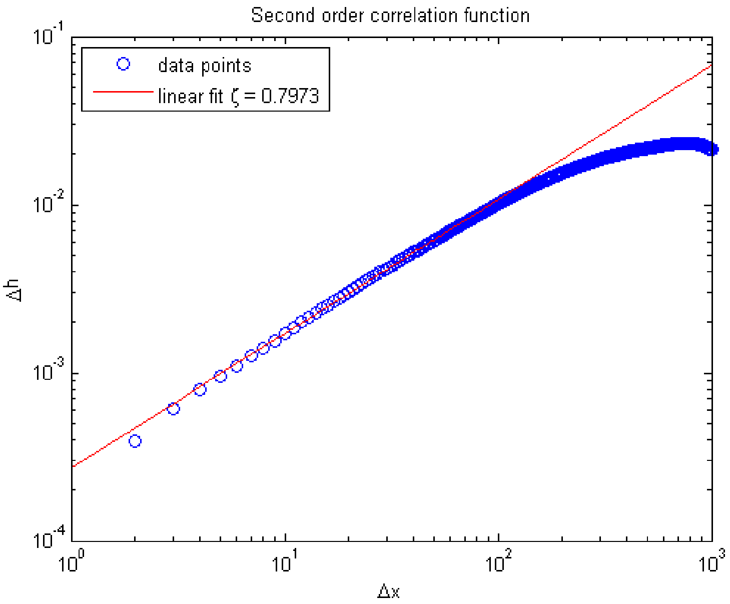

Figure A.2: Second order correlation function calculated along the x-axis. ζ is the slope of the red line. The unit along the x-axis is pixels, i.e. the bandwith Δx in number of pixels. The pixel size is 25 μm × 25 μm, so the unit along the x-axis is 25 μm.

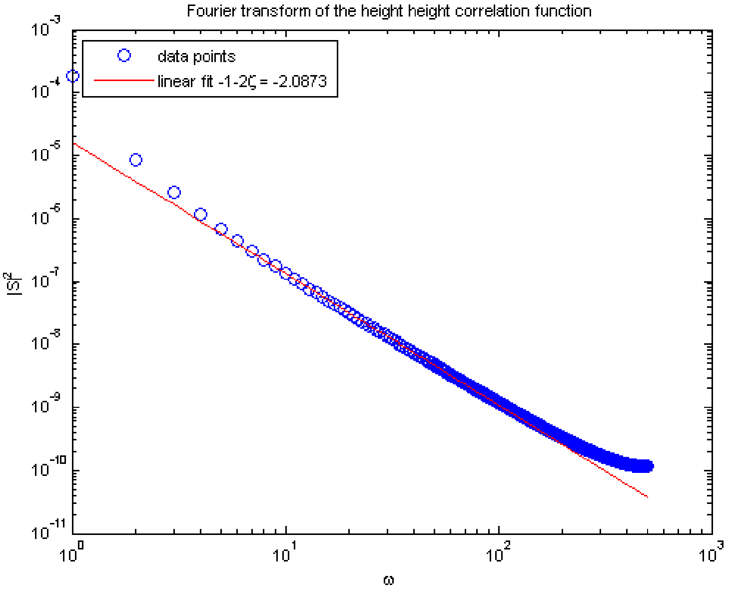

Figure A.3: Fourier transform of the height-height correlation function calculated along the x-axis. The slope of the red line is $-(1+2\zeta)$ which corresponds to $\zeta = 0.54$.

Figures A.1 to A.3 show the data analysis along the x-axis[1].

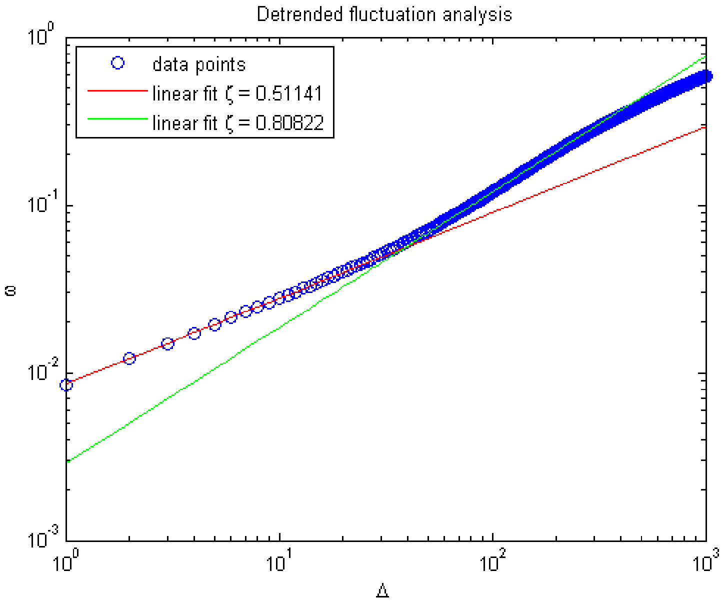

Figure A.4: Detrended fluctuation analysis calculated along the y-axis. Each ζ is the slope of each of the red and green lines. The unit along the x-axis is pixels, i.e. the bandwith Δ in number of pixels. The pixel size is 25 μm × 25 μm, so the unit along the x-axis is 25 μm.

---

[1] The x-axis is not refering to the horizontal axis in the plot, but the direction in which the fracture has propagates

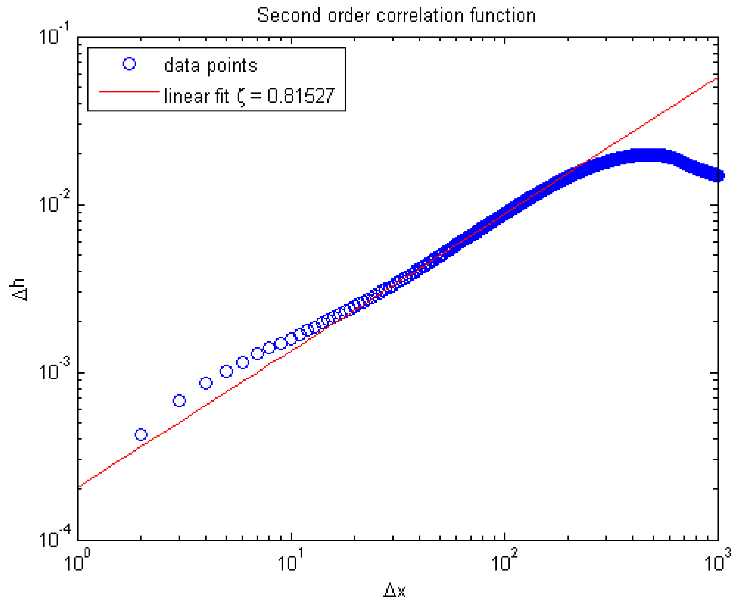

Figure A.5: Second order correlation function calculated along the x-axis. ζ is the slope of the red line. The unit along the x-axis is pixels, i.e. the bandwith Δx in number of pixels. The pixel size is 25 μm × 25 μm, so the unit along the x-axis is 25 μm.

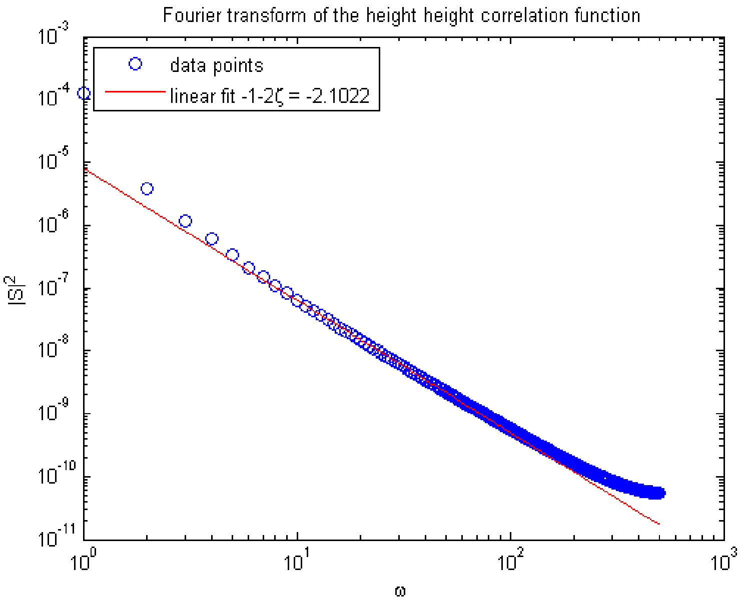

Figure A.6: Fourier transform of the height-height correlation function calculated along the x-axis. The slope of the red line is $-(1+2\zeta)$ which corresponds to $\zeta = 0.55$. The unit along the x-axis is pixel^{-2}

The roughness exponents for all the plots are given in Table A.1

Table A.1: Calculated roughness exponents taken from the plots.

Figure number	ζ
A.1	0.69
A.2	0.80
A.3	0.54
A.4	0.51 (0.81)
A.5	0.82
A.6	0.55

Figures A.4 to A.6 show the data analysis along the y-axis. It is interesting to notice the two linear fits made for the detrended fluctuation analysis in the direction perpendicular to the fracture propagation direction shown in Figure A.4. Here, a crossover between two scaling regimes is very clearly shown, like Henrik Hemmen also found. The two straight lines cross somewhere between the values 30 and 40 which is equivalent to a bandwidth a little smaller than Δ = 1 mm. However, this cannot clearly be seen on the other plots. Nevertheless, it can seem as Henrik Hemmen's argument regarding the data initially obtained from Professor Schmittbuhl applies to this data as well; that the measurements are made on the crossover and that the roughness exponent found for that reason will be somewhere between the smaller and the larger scaling regimes. Further investigation is however required before any conclusions can be drawn. Figure A.7 is taken from Henrik Hemmen's master's thesis [16]. He found a roughness exponent around 0.5 with the MRI data, while the laser profilometry measurement shows a crossover from $\zeta = 0.3$ to $\zeta = 0.8$.

As a test, the same analysis as above was done with just one 8th of the laser profilometry data points, in order to compare laser profilometry data with the MRI data with similar resolution. The results are shown in Figures A.8 and A.9. The roughness exponent found directly by the plots was 0.53 [16], but this doesn't compare very well with the 0.64 and 0.73, so it seems clear that no conclusions can be drawn untill further investigations have been performed.

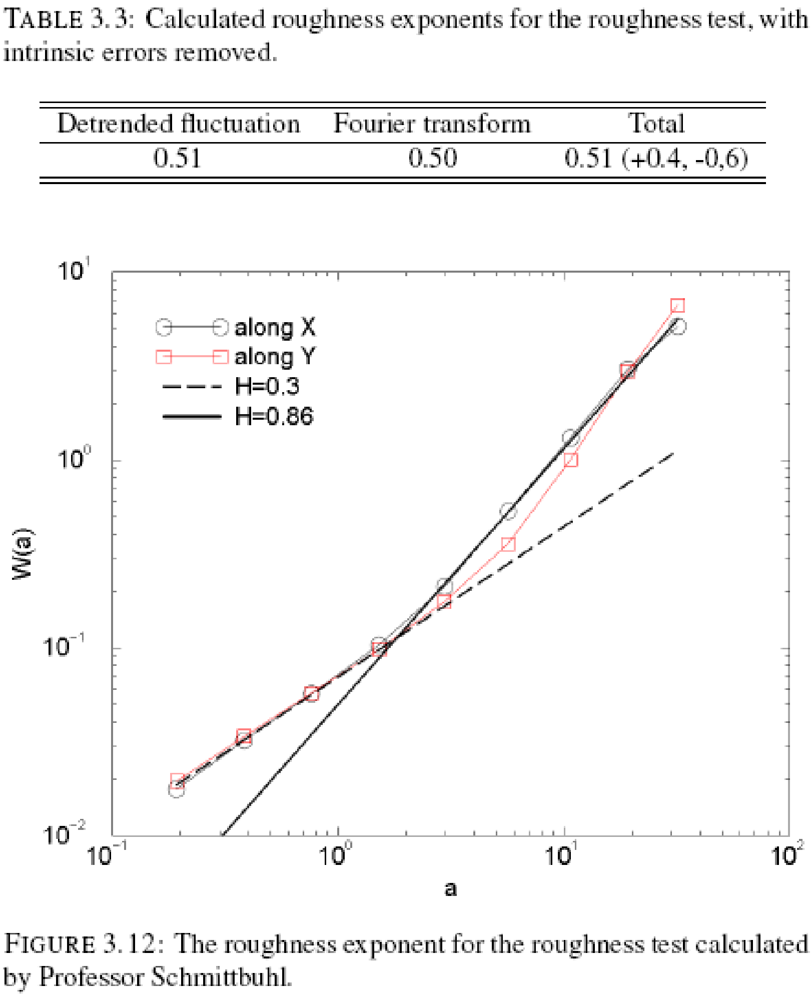

TABLE 3.3: Calculated roughness exponents for the roughness test, with intrinsic errors removed.

Detrended fluctuation	Fourier transform	Total
0.51	0.50	0.51 (+0.4, -0,6)

FIGURE 3.12: The roughness exponent for the roughness test calculated by Professor Schmittbuhl.

Figure A.7: Results from Henrik Hemmen's master's thesis, showing results from the MRI data in the table and from the laser profilometry measurements in the plot beneath. The numbers in the table have been obtained by compensating for intrinsic errors.

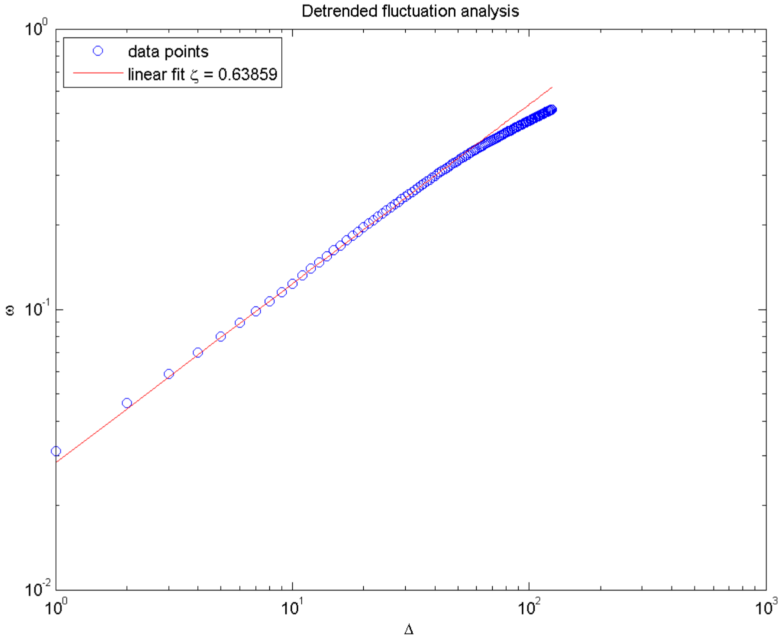

Figure A.8: Detrended fluctuation analysis calculated along the x-axis. The unit along the x-axis is pixels, i.e. the bandwith Δ in number of pixels. The pixel size is 0.2 mm × 0.2 mm, so the unit along the horizontal axis is 0.2 mm.

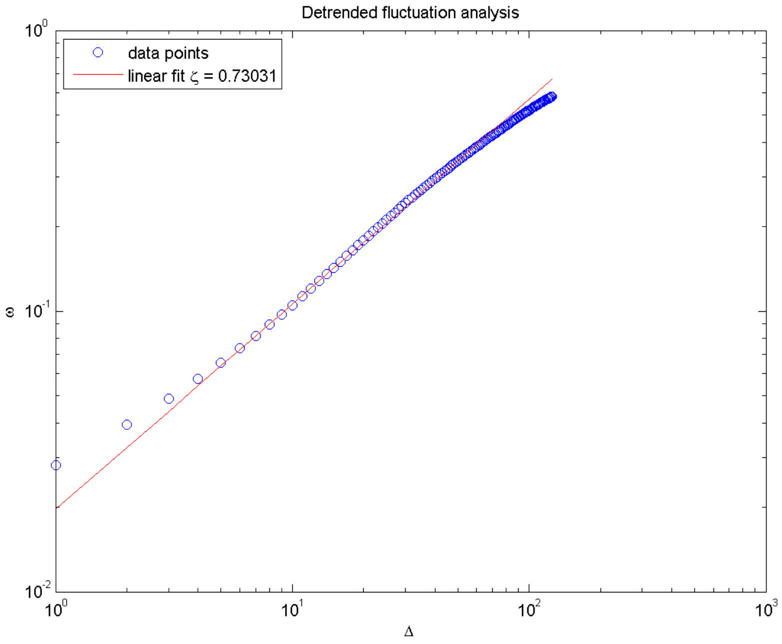

Figure A.9: Detrended fluctuation analysis calculated along the y-axis. The unit along the x-axis is pixels, i.e. the bandwith Δ in number of pixels. The pixel size is 0.2 mm × 0.2 mm, so the unit along the horizontal axis is 0.2 mm.